JOURNAL OF PETROLOGY

Journal of Petrology, 2016, Vol. 57, No. 8, 1509–1530
doi: 10.1093/petrology/egw048
Original Article

OXFORD

Spatio-temporal Geochemical Evolution of the SE Australian Upper Mantle Deciphered from the Sr, Nd and Pb Isotope Compositions of Cenozoic Intraplate Volcanic Rocks

K. F. Oostingh[1]*, F. Jourdan[1], R. Merle[2] and M. Chiaradia[3]

[1]Department of Applied Geology and JdL Centre, Curtin University, Perth, WA 6845, Australia; [2]Research School of Earth Sciences, The Australian National University, Canberra, ACT 0200, Australia and [3]Section des Sciences de la Terre, University of Geneva, 13 Rue de Maraîchers, 12011, Geneva, Switzerland

*Corresponding author. Present address: Department of Applied Geology, Curtin University, GPO Box U1987, Perth, WA 6845, Australia. E-mail: k.oostingh@postgrad.curtin.edu.au

Received October 15, 2015; Accepted July 28, 2016

ABSTRACT

Intraplate basaltic volcanic rocks ranging in age from Late Cretaceous to Holocene are distributed across southeastern Australia in Victoria and eastern South Australia. They comprise four provinces differentiated on the basis of age and spatial distribution. The youngest of these (<4·6 Ma) is the Newer Volcanic Province (NVP), which incorporates lava flows, scoria cones and maars, distributed across western and central Victoria into South Australia. The oldest eruptive rocks belong to the 95–19 Ma Older Volcanic Province, which comprises basaltic lava flows and shallow intrusions distributed across eastern and central Victoria. When examined within the broader framework of geochemical data available for Cretaceous to Cenozoic intraplate volcanism in southeastern Australia, new major, minor and trace element and Sr, Nd and Pb isotope analyses of volcanic rocks from the NVP suggest that their parental magmas originated from a distinctively different mantle source compared with that of the Older Volcanics. We propose that the magmas represented by the Older Volcanics originated from low degrees of partial melting of a mixed source of Indian mid-ocean ridge basalt (MORB)-source mantle and calcio-carbonatite metasomatized subcontinental lithospheric mantle (SCLM), followed by up to 20% fractional crystallization. The magmas of the youngest (<500 ka) suite of the NVP (the Newer Cones) were generated by up to 13% partial melting of a garnet-rich source, followed by similar degrees of fractional crystallization. We also suggest that the temporally intermediate Euroa Volcanics (~7 Ma) reflect chemical evolution from the source of the Older Volcanics to that of the Newer Cones. Furthermore, energy-constrained recharge, assimilation and fractional crystallization (EC-RA$_x$FC) modelling suggests that the Sr isotope signature of the ~4·6–1 Ma Newer Plains component of the NVP can be explained by up to 5% upper crustal assimilation. On the basis of these results and data from the literature for mantle xenoliths, we propose a geodynamic model involving decompression melting of metasomatized veins at the base of the SCLM generating the Older Volcanics and modifying the ambient asthenosphere of Indian MORB isotope character. This was followed by thermal erosion and entrainment of the resulting depleted SCLM into the modified Indian MORB-source asthenospheric mantle, generating the Newer Cones. Such a model is in agreement with recent geophysical observations in the area suggesting edge-driven convection with shear-driven upwelling as a potential geodynamic model resulting in temporal upwelling in the region.

Key words: Newer Volcanic Province; SE Australia; basalt; intraplate volcanism

INTRODUCTION

Cainozoic intraplate volcanism in SE Australia was initiated during the breakup of Gondwana and subsequent rapid northward rifting of the Australian plate from 40 Ma onward (Veevers, 1986). In Victoria and South Australia, volcanism is represented by the 95–19 Ma Older Volcanics and the eruptive products of the Newer Volcanic Province (NVP; Fig. 1), comprising the 4·5–1 Ma Newer Plains and the <1 Ma Newer Cones. A 10–5 Ma volcanic field of similar age to the largely felsic rocks of the Macedon–Trentham volcanic province (Price *et al.*, 2003) and with spatial affinities to both the westernmost Older Volcanics and the easternmost Newer Volcanics is located near the town of Euroa [Fig. 1; hereafter referred to as the Euroa Volcanics after Paul *et al.* (2005)]. The NVP is subdivided into two distinct regions based on geomorphology: the Central Highlands and Western Plains (Fig. 1). The presence of hot springs (Cartwright *et al.*, 2002) suggests that the province is still active. Nevertheless, the source and provenance of the Older Volcanics, the Newer Plains and Newer Cones basalts are still a matter of debate (O'Reilly & Zhang, 1995; Price *et al.*, 1997, 2014; Zhang *et al.*, 1999; Demidjuk *et al.*, 2007). Enriched geochemical signatures for the Newer Plains eruptive rocks, which have spatially variable Sr isotope compositions corresponding to the location of both the Moyston Fault and the Selwyn Block (Fig. 1), led Price *et al.* (1997, 2014) to suggest that the lithosphere had an important control on the observed geochemical variation within the series. It is now well established that the region is underlain by a complex Palaeozoic basement (Cayley *et al.*, 2011) as well as metasomatized and heterogeneous sub-continental lithospheric mantle (SCLM) (Griffin *et al.*, 1988; O'Reilly & Griffin, 1988; Stolz & Davies, 1988; Yaxley *et al.*, 1991; Handler *et al.*, 1997). Pb isotope systematics may be able to resolve mantle source variations at much higher resolution than Sr and Nd isotope and trace element systematics (e.g. Ewart, 2004); however, Pb isotope data are available only for basalts of the Older Volcanics (Price *et al.*, 2014), the suite of volcanic rocks around the town of Euroa (Paul *et al.*, 2005) and two eruption centres of the Newer Cones–Mt Rouse (Boyce *et al.*, 2015) and Mt Gambier (Van Otterloo *et al.*, 2014). However, single eruptions typically represent discrete and compositionally distinct magma batches, resulting in considerable geochemical variation within and between eruption centres, stressing the need for larger scale geochemical investigations to understand the processes involved in monogenetic volcanism (McGee *et al.*, 2013). Here, we present new major and trace element and Pb, Sr and Nd isotope data for 11 volcanic centres, and their associated flows, of the Newer Cones, which, with a relatively young age span from around 500 000 to 5000 years (Blackburn *et al.*, 1982; Matchan & Phillips, 2011, 2014), represent a proxy for the current geochemical composition of the mantle beneath SE Australia. Recent ultra-precise $^{40}Ar/^{39}Ar$ age dating of these samples confirms their young age, and exemplifies the major age difference between the ~4 Ma Newer Plains (Gray & McDougall, 2009) and the <500 ka Newer Cones in the NVP (Oostingh *et al.*, 2015). Combined data from the Older Volcanics, Euroa Volcanics and the Newer Plains and Newer Cones allow us to resolve spatial and temporal source variations and differences in magmatic processes to elucidate the origin of SE Australian Cenozoic magmatism.

OVERVIEW OF CENOZOIC MAGMATISM IN SE AUSTRALIA

Older Volcanics

Day (1983, 1989) subdivided the limited outcrops of the Older Volcanics (Fig. 1b) into 15 separate fields on the basis of their major and trace element compositions and outcrop distribution. There is a continuum of compositions from nephelinite to quartz-tholeiitic basalt, showing no spatial and temporal correlation between basalt type and location or age. Even though K–Ar dating suggests that volcanism was almost continuous from 95 to 19 Ma (Wellman, 1974), single volcanic fields show a more restricted age range, leading Day (1983, 1989) to subdivide the Older Volcanics into four groups: Group 1 (95–55 Ma), Group 2 (59–38 Ma), Group 3 (44–31 Ma) and Group 4 (29–19 Ma). Recently published major and trace element and Sr, Nd and Pb isotope data (Price *et al.*, 2014) suggest that the Older Volcanics were derived from a three-component source involving depleted mantle (DM) and enriched (EMI and EMII) mantle components. Enrichment in incompatible trace elements and light rare earth elements (LREE) over heavy rare earth elements (HREE) in the Older Volcanics can be explained by partial melting of a heterogeneous mantle source followed by limited fractional crystallization and minor crustal assimilation (Price *et al.*, 2014). Price *et al.* also recognized two groups of high Mg-number samples that exhibit subtle variations in their trace element characteristics, potentially derived from depleted mantle mixing with different metasomatized components (either 2–3% EMI or 1% calcio-carbonatite).

Euroa Volcanics

The Euroa region represents a key location, as it has spatial affinities with both the Older Volcanics and Newer Plains and Newer Cones basalts, as well as the small felsic flows, domes, plugs and spines of the Macedon–Trentham region (Paul *et al.*, 2005; Fig. 1b) and is located on a north–south trend of more felsic magmatism (8–5 Ma; Wellman & McDougall, 1974). These more evolved rocks (mugearite to trachyte) have been previously interpreted as the southernmost extent of the New South Wales leucitite suite, a north–south-trending linear chain of volcanic centres proposed as a trace of hotspot volcanism (Nelson *et al.*, 1986; Davies

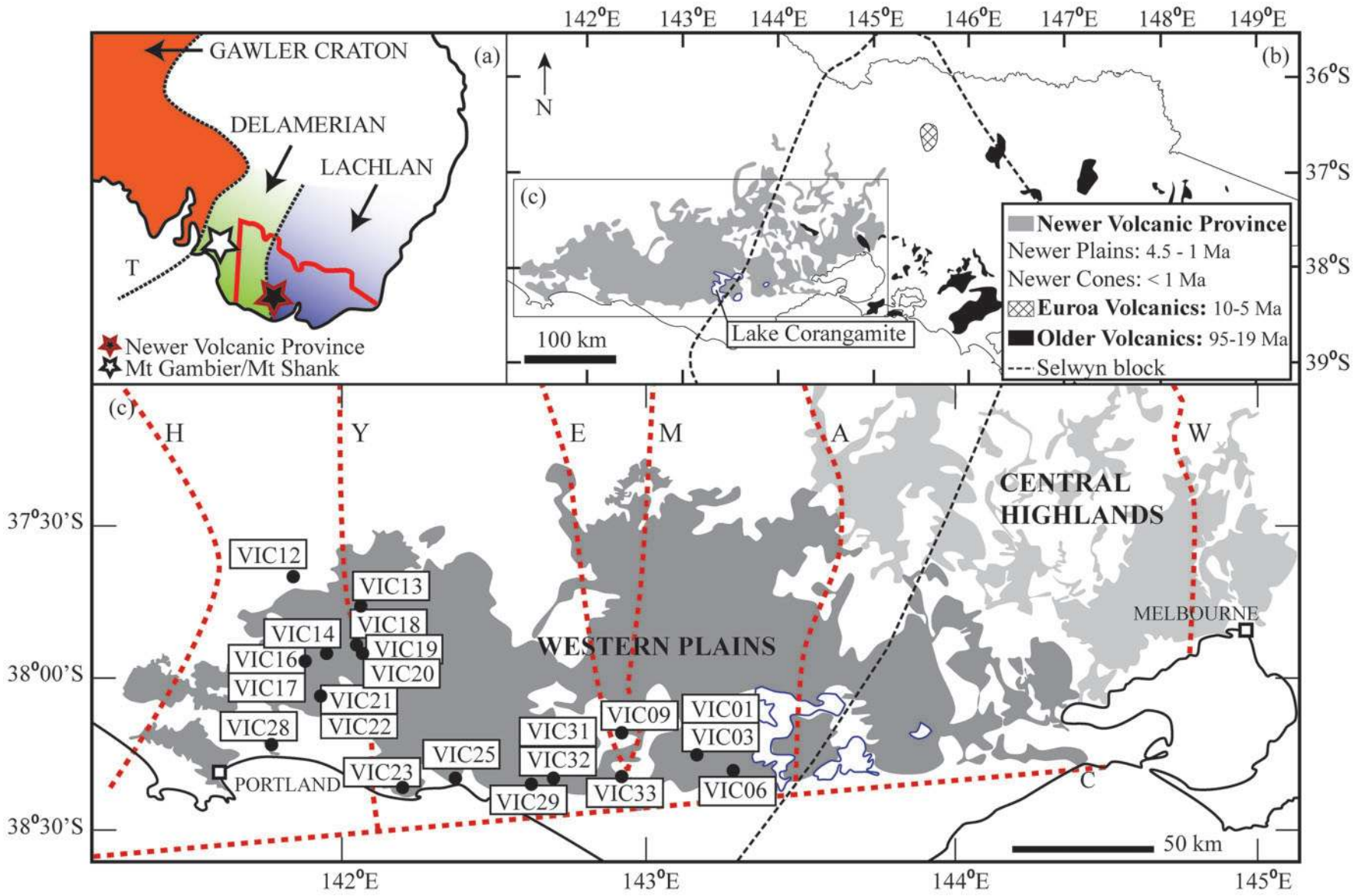

Fig. 1. (a) Location of the Newer Volcanic Province in Victoria and its youngest expression (Mt Gambier and Mt Shank) in South Australia. The Tasman Line (T), the Gawler Craton, as well as the Delamerian and Lachlan fold belts are indicated. (b) Enlarged section of (a) indicating the approximate extent of the Newer Volcanics Province in grey; the 4·5–1 Ma Newer Plains are located stratigraphically below the <1 Ma Newer Cones. The 10–5 Ma Euroa Volcanics are indicated by cross-hatching. The 95–19 Ma Older Volcanics are indicated in black. The dashed line represents the approximate outline of the Selwyn Block at depth (Cayley *et al.*, 2011). (c) Simplified outcrop of the volumetrically dominant Western Plains sub-province indicated in dark grey and location of samples. Indicated in light grey is the Central Highlands sub-province; this is an area of slightly older volcanism (Aziz-ur-Rahman & McDougall, 1972). The black dashed line represents the approximate westernmost outline of the Selwyn block at depth. Major faults are indicated by dashed red lines: C, Colac lineament; H, Hummocks fault; Y, Yarramyljip fault; E, Escondida fault; M, Moyston fault; A, Avoca fault; W, Mt William fault.

et al., 2015). However, work by Paul *et al.* (2005) revealed that the geochemical characteristics of the Euroa Volcanics are distinct from the New South Wales leucitites, questioning the extension of potential hotspot-related extrusive rocks into Victoria. Geochemical similarities of the Euroa Volcanics to both the Older Volcanics and Newer Plains and Newer Cones basalt suites (Price *et al.*, 2014) suggest a common source. Their age range and location provide an additional constraint on the temporal and spatial variability of this source and magmatic processes.

Newer Volcanics

The youngest expressions of intraplate volcanism are the <4·6 Ma (McDougall *et al.*, 1966; Aziz-ur-Rahman & McDougall, 1972; Gray & McDougall, 2009) alkaline basaltic volcanic products of the Newer Plains and Newer Cones series in the NVP (Fig. 1a and b) covering around 15 000–20 000 km^2 of Victoria and South Australia (Price *et al.*, 2003; Boyce, 2013) and comprising more than 704 eruption points from >416 volcanic centres (Boyce, 2013). In the Central Highlands sub-province, scoria cones and lava shield volcanoes have produced valley flows and small lava plains. In the volumetrically dominant Western Plains sub-province, thin, ~4·6–1 Ma lava flows (Gray & McDougall, 2009; termed the Newer Plains) cover a basement of Palaeozoic sediments and granite, whereas a younger (<10–300 ka; Aziz-ur-Rahman & McDougall, 1972) volcanic phase is characterized by small (<100 m high) scoria cones, maars and lava shields with associated flows (termed the Newer Cones; Price *et al.*, 2003). These Newer Cones eruptive rocks are alkalic in composition and have strong incompatible element enrichment, whereas the underlying Newer Plains eruptive rocks comprise less enriched transitional to tholeiitic rock types (Price *et al.*, 2003).

GEOLOGICAL SETTING AND SAMPLE DESCRIPTIONS

The NVP is restricted between 141 and 145°E and 37 and 38·5°S, and is underlain by a complex Palaeozoic basement consisting of a series of eastward younging, stacked fold belts of deformed and metamorphosed rocks of the Delamerian and Lachlan orogenies, occurring east of the Tasman Line, which subdivides the Palaeozoic basement from the Proterozoic Gawler Craton (Fig. 1a). An important structural domain is the early Ordovician continental crust of the inferred Selwyn basement block within the southern Lachlan Orogen (Cayley *et al.*, 2011), which underlies most of the Older Volcanics, but is absent from the basement below our samples of the Newer Volcanics of the Western Plains that were sampled west of Lake Corangamite (Fig. 1b).

We focused our sampling efforts on the volumetrically dominant Western Plains sub-province in the NVP, targeting the young Newer Cones. Although extensive literature data are available on the petrology and major and trace element geochemistry of these Newer Cones (see Price *et al.*, 2003, and references therein), isotope data are scarce. A recent study by Price *et al.* (2014), as well as work by Paul *et al.* (2005), reported isotope data for the Older Volcanics, Newer Plains and Euroa Volcanics. This highlights the need for an updated dataset for the Newer Cones to expand the current isotope geochemical database available for localized volcanic centres (Van Otterloo *et al.*, 2014; Boyce *et al.*, 2015). We targeted young scoria cones and lava shields and their flows at Mt Leura (VIC03), Mt Porndon (VIC06), Mt Noorat (VIC09), Mt Pierrepoint (VIC13), Mt Napier (VIC18, VIC19 and VIC20) and its Harman flow (VIC14, VIC16 and VIC17), the flow from Mt Rouse (VIC23), the Tower Hill complex (VIC25), Mt Eccles (VIC21 and VIC22) and its Tyrendarra flow (VIC28) and Staughton Hill (VIC33), as well as a smaller, as yet unnamed cone GEOVIC ME-2 (Boyce, 2013; VIC31 and VIC32) which we will refer to subsequently as Mt Boomerang, and the flow at Hopkins Falls that cannot be linked to a clear eruptive centre (VIC29). Samples are typically dark grey, cryptocrystalline basalt with fresh plagioclase laths and fresh olivine visible in hand specimen and minor vesicularity; in the case of flows, vesicles are commonly aligned. Samples VIC19 and VIC22 represent scoriaceous samples with a very fine, glassy groundmass, whereas VIC25 represents a volcanic bomb within tuff layers at the Tower Hill complex. Mantle xenoliths (centimetre-scale) are present in samples VIC03, VIC09 and VIC31 and VIC32 and olivine glomerocrysts occur in samples VIC29 and VIC33. All samples are devoid of any alteration in thin section. The principal mineral phases observed are phenocrysts of olivine, plagioclase and clinopyroxene in groundmass containing laths of plagioclase and Fe–Ti oxides.

METHODS

Samples were pulverized in an agate pestle and mortar. The major, minor and trace element contents of 20 samples were analysed for major elements at Intertek Genalysis Laboratories, Perth, using X-ray fluorescence (XRF), followed by standard dissolution techniques and analysis of solutions for trace elements by inductively coupled plasma mass spectrometry (ICP-MS). Internal standards SARM1 and SY-4 were used for the major elements and SY-4, OREAS25a, OREAS25b and GBW07105 for the trace elements. All major (XRF) and trace element (ICP-MS) analyses have an internal and external precision better than 5% at the 95% confidence level (2σ), except for V and Zr, which show precision >5% (2σ) for the standards reported.

Strontium, Nd and Pb isotopes were analysed on a subset of nine samples at the Department of Earth Sciences (University of Geneva, Switzerland) using the method described by Chiaradia *et al.* (2011) and a Thermo Neptune PLUS multi-collector ICP-MS system in

Table 1: Major (wt %) and trace element (ppm) analyses of Newer Volcanic Province basalts

Location:	VIC03 Mt Leura	VIC06 Mt Porndon	VIC09 Mt Noorat	VIC12 Wannon Falls	VIC13 Mt Pierre-point	VIC14 Harman flow	VIC16 Harman flow	VIC17 Harman flow	VIC18 Mt Napier	VIC19 Mt Napier
Lat. (°):	–38·25	–38·30	–38·18	–37·67	–37·77	–37·92	–37·94	–37·94	–37·89	–37·89
Long. (°):	143·16	143·28	142·92	141·84	142·06	141·95	141·88	141·88	142·05	142·05
Major elements (wt %)										
SiO_2	44·06	50·68	46·87	49·57	51·19	49·62	48·54	48·88	50·02	50·47
Al_2O_3	12·86	13·97	14·11	14·45	14·21	14·50	13·78	13·57	15·28	15·42
TiO_2	3·22	2·13	2·76	1·88	1·83	1·82	2·09	2·03	2·34	2·32
Fe_2O_3	14·37	12·23	13·20	11·65	11·53	12·23	12·29	12·16	11·71	11·46
MnO	0·17	0·16	0·17	0·15	0·15	0·15	0·16	0·16	0·15	0·15
MgO	9·72	8·05	7·45	9·27	8·07	7·76	9·94	10·21	6·75	6·46
CaO	8·34	8·46	7·37	8·40	8·41	8·66	8·98	8·98	8·29	8·45
Na_2O	4·37	3·48	4·96	3·51	3·45	3·45	3·21	3·30	4·09	3·91
K_2O	2·26	1·16	2·76	1·16	0·92	0·92	1·08	1·13	1·39	1·39
Cr_2O_3	0·04	0·04	0·03	0·04	0·05	0·04	0·05	0·05	0·02	0·02
P_2O_5	1·29	0·44	1·02	0·41	0·33	0·33	0·45	0·43	0·50	0·43
LOI	–0·69	–0·59	–0·83	–0·35	0·02	0·25	–0·34	–0·65	–0·52	–0·44
Total	100·10	100·30	100·00	100·18	100·19	99·77	100·28	100·30	100·06	100·09
Mg-no.	61	61	57	65	62	60	65	66	57	57
Trace elements (ppm)										
Rb	51·1	27·6	48·4	19·8	17·9	14·8	14·7	20·6	28·0	25·7
Ba	590·4	240·8	557·9	296·6	267·8	258·1	307·6	303·4	342·2	368·6
Th	6·4	3·1	7·1	2·8	2·2	2·1	2·8	2·8	3·0	3·2
Nb	78·2	28·8	77·8	31·7	25·2	23·5	30·2	29·2	34·3	34·2
Sr	1044·3	477·0	1095·6	670·4	466·5	475·1	529·9	536·5	609·9	627·4
Hf	7·9	4·6	9·0	4·1	3·6	3·3	3·7	3·6	4·3	4·6
Zr	311	166	363	154	138	124	142	135	169	176
Y	26·2	21·6	23·4	19·9	20·6	19·8	19·1	19·1	21·4	21·9
Pb	5·3	2·8	6·7	2·1	2·7	1·9	2·1	3·4	2·3	2·7
Ta	4·7	1·7	5·2	1·9	1·5	1·5	1·8	1·7	2·1	2·1
U	1·8	0·9	2·0	0·6	0·5	0·1	0·7	0·6	0·7	0·8
Sc	13·0	18·0	11·0	19·0	18·0	18·0	19·0	18·0	15·0	16·0
V	197	185	161	180	153	171	192	188	192	191
Cr	236	245	176	285	308	286	293	304	101	103
Co	63·5	49·1	49·4	53·7	51·5	55·7	55·0	56·5	43·4	62·1
Ni	230·8	149·0	157·1	195·2	209·0	214·4	216·6	224·1	109·0	101·8
La	65·0	23·3	59·5	22·5	18·1	17·8	21·3	22·1	25·0	25·6
Ce	133·8	49·0	117·7	44·8	37·3	35·7	45·1	44·0	49·9	50·7
Pr	15·5	6·2	14·2	5·5	4·8	4·5	5·6	5·4	6·3	6·2
Nd	62·9	26·0	54·7	23·5	20·5	18·9	24·0	23·0	25·5	27·3
Sm	12·0	6·1	10·7	5·3	5·0	4·7	5·3	5·3	5·8	5·9
Eu	4·1	2·0	3·5	1·8	1·7	1·7	1·9	1·8	2·1	2·1
Gd	10·3	6·0	9·5	5·1	5·2	5·2	5·5	5·3	6·1	6·0
Tb	1·3	0·9	1·3	0·8	0·8	0·7	0·8	0·8	0·8	0·9
Dy	6·5	4·9	5·8	4·1	4·2	4·2	4·2	4·1	4·5	4·7
Ho	1·1	0·8	1·0	0·7	0·8	0·8	0·8	0·7	0·8	0·8
Er	2·4	2·3	2·2	2·0	2·0	2·0	1·9	1·9	2·1	2·1
Tm	0·3	0·3	0·3	0·2	0·2	0·3	0·2	0·2	0·3	0·3
Yb	1·6	1·7	1·3	1·3	1·4	1·5	1·6	1·6	1·6	1·6
Lu	0·2	0·2	0·2	0·2	0·2	0·2	0·2	0·2	0·2	0·2

(continued)

static mode. Ratios used for internal fractionation were $^{88}Sr/^{87}Sr = 8{\cdot}375209$ for $^{87}Sr/^{86}Sr$, $^{146}Nd/^{144}Nd = 0{\cdot}7219$ for $^{143}Nd/^{144}Nd$ and $^{203}Tl/^{205}Tl = 0{\cdot}418922$ for the three Pb isotope ratios (a Tl standard solution was added to the sample). The ^{144}Sm interference on ^{144}Nd was monitored on mass ^{147}Sm and corrected by using a $^{144}Sm/^{147}Sm$ value of 0·206700, and ^{204}Hg interference on ^{204}Pb was corrected by monitoring ^{202}Hg. External standards used were SRM987 ($^{87}Sr/^{86}Sr = 0{\cdot}710248$, long-term external reproducibility 10 ppm), JNdi-1 [$^{143}Nd/^{144}Nd = 0{\cdot}512115$ (Tanaka *et al.*, 2000), long-term external reproducibility 10 ppm], and SRM981 (Baker *et al.*, 2004) for Pb (long-term external reproducibility of 0·0048% for $^{206}Pb/^{204}Pb$, 0·0049% for $^{207}Pb/^{204}Pb$ and 0·0062% for $^{208}Pb/^{204}Pb$). Based on the systematic discrepancy between the measured and accepted Sr, Nd and Pb isotope ratios for the above standards, sample values were further corrected for external fractionation by a value of –0·039‰, +0·047‰ and +0·5‰ a.m.u., respectively.

RESULTS

All our new analyses of Newer Cones samples have loss on ignition (LOI) < 2 wt % (Table 1). Major element data have been normalized to 100% on a volatile-free

Table 1: Continued

Location:	VIC20 Mt Napier	VIC21 Mt Eccles	VIC22 Mt Eccles	VIC23 Mt Rouse flow	VIC25 Tower Hill	VIC28 Tyrendarra flow	VIC29 Hopkins Falls	VIC31 GEOVIC ME-2	VIC32 GEOVIC ME-2	VIC33 Staughton Hill
Lat. (°):	–37·92	–38·06	–38·06	–38·36	–38·33	–38·22	–38·35	–38·33	–38·33	–38·32
Long. (°):	142·07	141·93	141·93	142·20	142·37	141·77	142·62	142·69	142·69	142·92
Major elements (wt %)										
SiO_2	49·93	46·16	46·87	48·11	46·44	48·20	46·70	45·47	45·56	46·51
Al_2O_3	14·64	14·09	13·35	14·15	13·78	14·11	13·19	13·19	13·18	12·88
TiO_2	2·24	2·60	2·36	2·29	2·46	2·22	2·45	2·81	2·76	2·40
Fe_2O_3	11·73	12·91	13·20	12·80	13·05	12·99	13·18	12·99	12·77	13·37
MnO	0·15	0·17	0·17	0·16	0·17	0·17	0·17	0·17	0·16	0·17
MgO	7·84	7·92	10·10	8·87	8·86	8·68	11·01	10·60	10·48	11·12
CaO	8·58	9·66	9·19	9·03	8·79	8·75	9·05	9·01	9·16	9·05
Na_2O	3·78	3·69	3·27	3·43	4·07	3·69	3·32	3·45	3·44	3·05
K_2O	1·34	1·62	1·44	1·15	2·17	1·51	1·37	1·77	1·77	1·33
Cr_2O_3	0·03	0·04	0·05	0·04	0·03	0·04	0·05	0·04	0·05	0·05
P_2O_5	0·48	0·85	0·61	0·45	0·82	0·58	0·58	0·62	0·62	0·57
BaO	0·05	0·05	0·04	0·04	0·06	0·05	0·05	0·05	0·05	0·04
SO_3	0·01	0·04	0·07	0·01	0·05	0·02	0·01	0·02	0·03	0·01
LOI	–0·74	0·32	–0·61	–0·43	–0·52	–0·74	–0·87	–0·11	0·07	–0·47
Total	100·06	100·11	100·11	100·10	100·24	100·26	100·25	100·08	100·10	100·09
Mg-no.	61	59	64	62	61	61	66	66	66	66
Trace elements (ppm)										
Rb	26·5	31·8	27·5	21·9	44·8	30·9	25·4	33·6	35·3	23·9
Ba	350·1	457·2	350·3	278·2	518·5	390·6	354·9	411·8	399·8	344·9
Th	2·9	4·2	3·2	2·8	5·3	3·7	3·0	4·3	4·6	2·7
Nb	33·0	56·1	39·0	32·7	61·7	45·6	38·4	51·8	52·3	37·1
Sr	578·1	959·0	661·2	592·6	876·4	670·8	677·8	709·3	717·7	587·7
Hf	4·2	5·4	4·3	4·4	7·3	5·2	4·5	5·7	6·0	4·5
Zr	160	228	169	173	279	202	168	224	225	171
Y	20·7	25·6	20·6	21·0	25·5	23·0	20·9	21·6	21·9	21·3
Pb	2·5	2·8	2·3	2·2	4·0	2·9	3·1	2·8	3·1	1·6
Ta	2·1	3·3	2·3	2·1	3·9	2·8	2·4	3·5	3·4	2·3
U	0·8	1·3	0·9	0·8	1·5	0·9	0·9	1·1	1·3	0·7
Sc	17·0	19·0	18·0	20·0	17·0	18·0	19·0	18·0	19·0	19·0
V	191	219	203	200	194	189	208	221	231	204
Cr	171	242	282	273	205	238	311	281	295	367
Co	48·6	49·1	60·2	55·9	53·1	49·8	62·2	63·3	60·5	64·4
Ni	137·9	136·9	228·8	175·7	174·1	166·3	245·6	231·8	213·9	276·7
La	24·6	43·2	29·4	24·5	47·8	33·5	29·2	36·9	37·1	27·3
Ce	49·4	86·4	59·2	50·8	96·6	66·8	60·7	73·5	74·0	56·0
Pr	6·2	10·2	7·2	6·3	11·5	8·1	7·6	8·9	8·8	7·1
Nd	26·3	43·2	30·5	26·2	46·0	32·9	31·4	35·2	36·6	29·1
Sm	5·8	8·6	6·6	5·8	8·8	6·7	6·6	7·3	7·4	6·3
Eu	2·1	2·9	2·3	2·0	3·0	2·4	2·3	2·4	2·5	2·3
Gd	5·7	8·6	6·4	5·7	7·9	7·0	6·4	7·2	6·9	6·4
Tb	0·8	1·1	0·9	0·8	1·1	0·9	0·9	0·9	0·9	0·9
Dy	4·5	5·6	4·8	4·5	5·7	4·9	4·6	5·0	4·9	4·7
Ho	0·8	1·0	0·8	0·8	1·0	0·9	0·8	0·9	0·9	0·8
Er	2·1	2·3	2·1	2·0	2·4	2·2	2·0	2·2	2·2	2·0
Tm	0·2	0·3	0·2	0·2	0·3	0·3	0·2	0·3	0·3	0·2
Yb	1·5	1·7	1·5	1·7	1·6	1·8	1·2	1·5	1·5	1·4
Lu	0·2	0·2	0·2	0·2	0·2	0·2	0·2	0·2	0·2	0·2

basis, reported in Supplementary Data Table A1 (major and trace elements); isotopic data are reported in Supplementary Data Table A2 (Sr, Nd and Pb isotopes) (supplementary data are available for downloading at http://www.petrology.oxfordjournals.org). For comparison, we have also used whole-rock major and trace element data from the GEOROC database and data from Price *et al.* (2014), Van Otterloo *et al.* (2014) and Boyce *et al.* (2015) for the Cretaceous and Cenozoic intraplate volcanic rocks of southeastern Australia. We have not used data for altered samples with LOI $>$ 3 wt % or without LOI recorded as the quality of the data cannot be assessed.

Major elements

On a total alkalis–silica (TAS) diagram (Fig. 2; Le Bas *et al.*, 1986), the data obtained from this study overlap with published data for the Newer Cones, with all samples except VIC06, VIC13 and VIC14 plotting above the alkaline–sub-alkaline division line of Irvine & Baragar (1971). Seventeen Newer Cones samples plot within the basalt and trachybasalt fields, with three samples (VIC03, VIC09 and VIC25) classifying as basanite based on CIPW norm calculation. Data for sample VIC09 (SiO_2 47·1 wt % and total alkalis 7·8 wt %) overlap with those previously published for Mt Gambier and Mt Shank

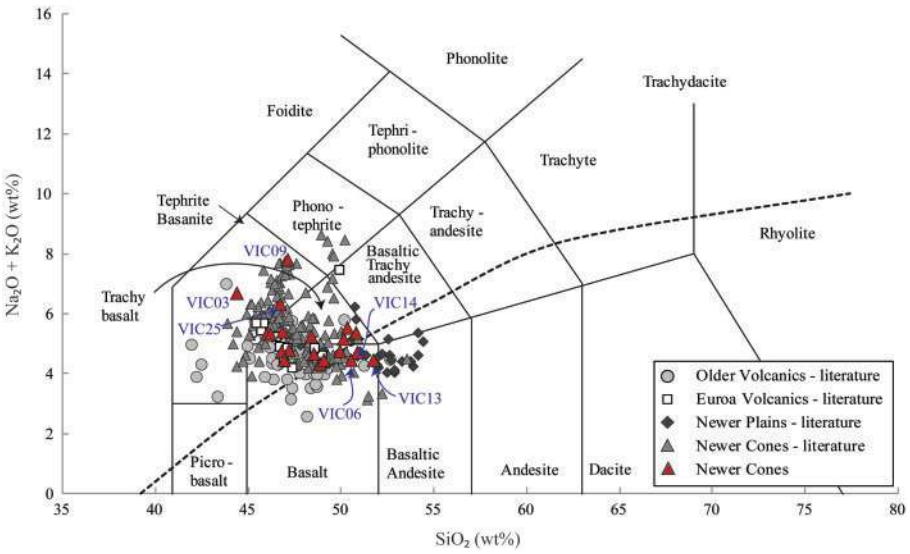

Fig. 2. Total alkalis–silica (TAS) diagram after Le Bas *et al.* (1986). Older Volcanics and Newer Plains data are from Price *et al.* (1997, 2014); Euroa Volcanics data are from Paul *et al.* (2005); Newer Cones literature data are from Frey *et al.* (1978), McDonough *et al.* (1985), Vogel & Keays (1997), Foden *et al.* (2002), Demidjuk *et al.* (2007), Van Otterloo *et al.* (2014) and Boyce *et al.* (2015). Dashed line represents the alkaline–sub-alkaline division of Irvine & Baragar (1971).

(Fig. 1a; McDonough *et al.*, 1985; Foden *et al.*, 2002; Demidjuk *et al.*, 2007), which represent the western-most and youngest suite of volcanic rocks of the NVP. Except for the three basanites, our analyses of the Newer Cones show a narrow range in $Na_2O + K_2O$ (wt %). Our samples define a positive covariation between Al_2O_3 concentration and Mg-number [atomic ratio of 100 Mg/(Mg + 0·85 Fe_{tot})] suggesting progressive differentiation, with our data overlapping the Al_2O_3 concentrations of literature data for the Newer Cones (Fig. 3a; Ellis, 1976; Frey *et al.*, 1978; McDonough *et al.*, 1985; Vogel & Keays, 1997; McBride *et al.*, 2001; Foden *et al.*, 2002; Demidjuk *et al.*, 2007; Van Otterloo *et al.*, 2014; Boyce *et al.*, 2015). Our samples show TiO_2 concentrations up to 3·2 wt %, which is lower than those reported for the youngest eruptive rocks in South Australia (Mt Watch and Mt McIntyre; McDonough *et al.*, 1985; Vogel & Keays, 1997; Foden *et al.*, 2002) (Fig. 3c). Our Newer Cones samples are also distinguished from these eruptive rocks by their lower CaO contents (7·4–9·8 wt %) (Fig. 3d).

Trace elements

Whole-rock Mg-numbers of our Newer Cones samples range between 57 and 66 and Ni, Cr and Co concentrations are in the range of 102–277 ppm, 101–367 ppm and 49–64 ppm, respectively. The samples show no trend in trace element contents versus Mg-number (Fig. 4a–f), except for a positive covariation in Ni concentration. This spread is mainly caused by basanite samples VIC03, VIC09 and VIC25, which are significantly enriched in incompatible trace elements such as La (47·8–65 ppm) and Rb (44·8–51·1 ppm) compared with the La (<37 ppm) and Rb (<34 ppm) concentrations in the other Newer Cones samples. Basanites excepted, our samples show a restricted range in trace element concentrations overlapping with literature data for other samples from this region, again except for the suite from Mt Schank and Mt Gambier (Foden *et al.*, 2002; Demidjuk *et al.*, 2007; Van Otterloo *et al.*, 2014). On a La/Nb vs Ba/Nb diagram the data cluster around the Primitive Mantle ratio (La/Nb 0·9 and Ba/Nb 9; Sun & McDonough, 1989; Fig. 4g). On a Ce/Pb vs Nb/U diagram, 18 of our 20 Newer Cones samples fall within the range defined for mid-ocean ridge basalts (MORB) and ocean island basalts (OIB) (Hofmann *et al.*, 1986; Fig. 4h), except for VIC14, which shows an extremely high Nb/U ratio of 235 owing to depletion of this sample in U (0·1 ppm vs >0·5 ppm for the other samples), and VIC06, which trends slightly towards the continental crust value (Taylor & McLennan, 1995). The samples show a typical OIB trace element signature on a normalized extended element diagram (Fig. 5) with relative enrichment of incompatible elements Rb, Ba, Th, U, Nb and LREE compared with primitive mantle, as well as negative Pb and positive Nb anomalies. The basanites (VIC03, VIC09 and VIC25) show a greater enrichment in LREE when compared with the trachybasalts and (sub-)alkaline basalts with La/Lu ratios (normalized to C1 chondrite) of >25. C1 chondrite-normalized REE patterns (Fig. 6; Sun & McDonough, 1989) furthermore show light rare earth element (LREE) vs middle rare earth element (MREE) and MREE/HREE enrichment for all Newer Cones samples.

Sr, Nd and Pb isotopes

Isotope ratios were corrected to initial values using new $^{40}Ar/^{39}Ar$ ages for the analysed samples (Oostingh *et al.*, 2015). For all samples, isotope age correction yields initial values that are indistinguishable from the

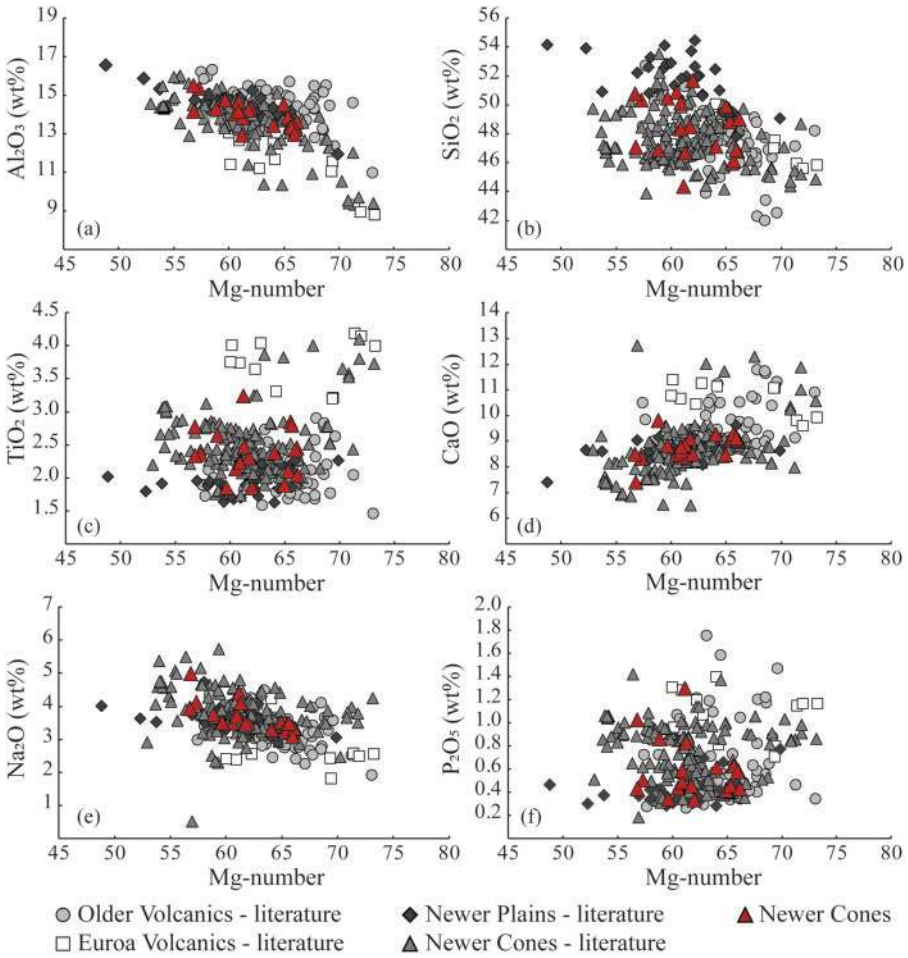

Fig. 3. Major element variation diagrams, all data normalized to 100% on a volatile-free basis. Mg-number calculated as the atomic ratio of [100Mg/(Mg + 0·85 Fe_{tot})]. Data sources as in Fig. 2.

measured values, with differences ranging between 0·00012% and 0·00001% from the analysed isotope composition. The samples define a relatively narrow range of $(^{87}Sr/^{86}Sr)_i$ from 0·70387 for VIC03 to 0·70424 for VIC25 (Table 2) for a wide range of Mg-numbers (Fig. 7), as well as a narrow range in $(^{143}Nd/^{144}Nd)_i$ ranging from 0·51281 to 0·51286. When plotted on a $(^{87}Sr/^{86}Sr)_i$ vs $(^{143}Nd/^{144}Nd)_i$ diagram, all samples are located within the mantle array (Fig. 8a), trending towards Bulk Silicate Earth (BSE; Zindler & Hart, 1986). Our samples show high $(^{207}Pb/^{204}Pb)_i$ and $(^{208}Pb/^{204}Pb)_i$ for a given $(^{206}Pb/^{204}Pb)_I$, ranging from 15·5472 to 15·6112 and from 38·4702 to 38·7449, respectively; $(^{208}Pb/^{204}Pb)_i$ shows a narrow spread over a wide range of Mg-number values, whereas $(^{207}Pb/^{204}Pb)_i$ and $(^{206}Pb/^{204}Pb)_i$ show similar trends but are slightly more scattered (Fig. 7). When plotted on $(^{206}Pb/^{204}Pb)_i$ vs $(^{207}Pb/^{204}Pb)_i$ and $(^{208}Pb/^{204}Pb)_i$ diagrams, most of the samples plot above and parallel to the Northern Hemisphere Reference Line (NHRL; Fig. 8b and c). When plotted on a $(^{207}Pb/^{204}Pb)_i$ vs $(^{143}Nd/^{144}Nd)_i$ diagram (Fig. 8d) it can be seen that the Newer Cones trend towards the HIMU mantle end-member, whereas the Older Volcanics trend towards EMII.

DISCUSSION

Geochemical comparison between the Newer Cones and the Older Volcanics, Euroa Volcanics and Newer Plains

Major and trace elements

The Newer Cones data overlap with those for the Older Volcanics and Euroa Volcanics in the alkaline field of the TAS diagram, whereas the Newer Plains show a more sub-alkaline geochemical composition (Fig. 2). All series show a wide range in major element compositions; in particular, a negative correlation between Al_2O_3 or Na_2O and MgO content and a slight positive correlation between CaO and Mg-number that indicates fractional crystallization of olivine and clinopyroxene without plagioclase (Fig. 3). Similar trends are observed for the Newer Cones, Newer Plains and the Older Volcanics. The Euroa Volcanics are distinct from the

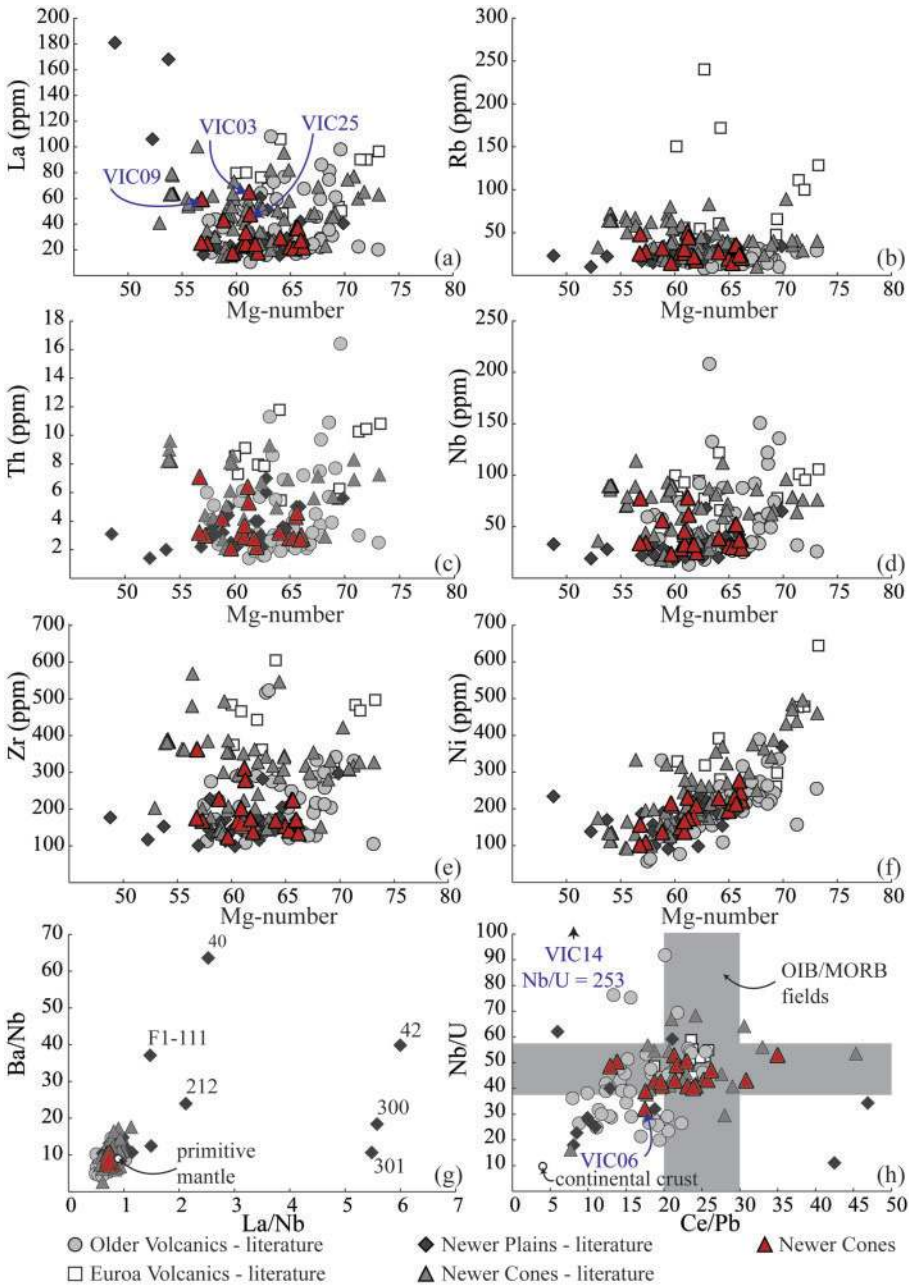

Fig. 4. (a–f) Trace element plots vs Mg-number for all series; data sources as in Fig. 2. Basanite samples VIC03, VIC09 and VIC25 are indicated in (a); (g): La/Nb vs Ba/Nb; the Primitive Mantle value is from Sun & McDonough (1989). Samples F1-111, 40, 42, 212, 300 and 301 (Price *et al.*, 1997) are indicated. (h) Ce/Pb vs Nb/U after Hofmann *et al.* (1986); the grey field represents the Ce/Pb (25 ± 5) and Nb/U (47 ± 10) ratios in both ocean island basalt (OIB) and mid-ocean ridge basalt (MORB); average continental crust is indicated (Nb/U = 10; Ce/Pb = 4; Taylor & McLennan, 1995).

other groups, having lower Al_2O_3 and Na_2O and higher MgO, TiO_2 and CaO contents similar to those of the Newer Cones in South Australia (Fig. 3).

Compared with the Newer Cones, the Euroa Volcanics are enriched in highly and moderately incompatible trace elements, with Rb contents up to ~240 ppm and Zr up to ~605 ppm. Whereas the Newer Plains generally show a restricted range in Mg-number and trace element composition, except for some outliers, the Older Volcanics display constant variation with Mg-numbers of 57–73 and a wide spread in trace element concentrations (Th 1·4–16·1 ppm, Zr 105–523 ppm, Nb 20–208 ppm), except for their narrow range of Rb concentrations of around 25 ppm (Fig. 4). Six Newer Plains samples (40, 42, 212, 300, 300 and F1-111; Price *et al.*, 1997) show extreme La/Nb enrichment of 1·5–6, with four of those (40, 42, 212 and F1-111) also having high Ba/Nb ratios of 23·95–63·58, suggestive of fluid metasomatism of their source (Price *et al.*, 1997). The other series show a gradual trend, with the Older Volcanics having the lowest La/Nb and Ba/Nb ratios (~0·5 and ~6 respectively; Fig. 4g), whereas the Euroa

Volcanics overlap with our Newer Cones data having La/Nb of ~0·7 and Ba/Nb of ~8, followed by the Newer Plains, which show the most extreme enrichment. All groups show enrichment in Ni (Fig. 4f) with increasing Mg-number. A major part of the Newer Plains as well as some of the Older Volcanics trend towards the average continental crust value (Taylor & McLennan, 1995) on a Ce/Pb vs Nb/U diagram (Fig. 4h), suggestive of crustal contamination. The Older Volcanics and the Euroa Volcanics have very similar OIB-type trace element characteristics, with negative Pb and positive Nb anomalies (Fig. 5). These anomalies are absent in some of the Newer Plains basalts, which instead show a positive U anomaly for some samples. Figure 6 shows that the Older Volcanics and Newer Plains have C1 chondrite-normalized REE patterns similar to those of the Newer Cones, whereas the Euroa Volcanics are characterized by greater LREE enrichment.

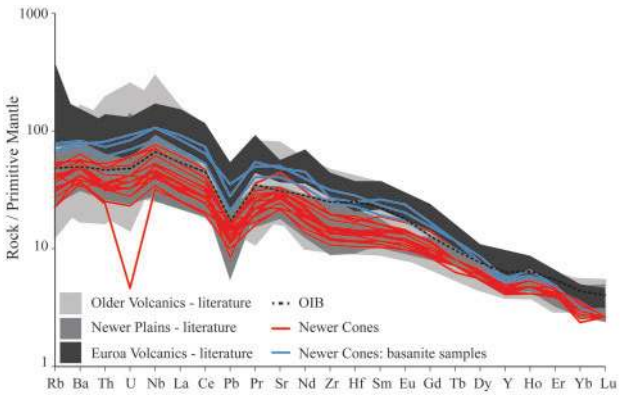

Fig. 5. Primitive mantle normalized trace element patterns for the Newer Volcanics compared with the Older Volcanics. Typical ocean island basalt (OIB; Sun & McDonough, 1989) is indicated with a black dashed line. Basanite samples VIC03, VIC09 and VIC25 indicated are indicated by blue lines. Data sources as in Fig. 2.

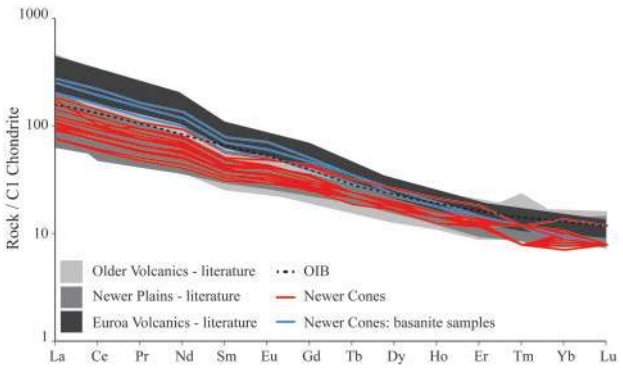

Fig. 6. Rare earth element (REE) C1 chondrite (Sun & McDonough, 1989) normalized patterns. Typical ocean island basalt (OIB; Sun & McDonough, 1989) is indicated with a black dashed line. Basanite samples VIC03, VIC09 and VIC25 are indicated by blue lines. Data sources as in Fig. 2.

Sr, Nd and Pb isotopes

Strontium and Nd isotope data for the Newer Cones overlap with published data (Fig. 7a and b). Our Pb isotope data overlap with the recently published data for Mt Rouse (Boyce *et al.*, 2015), a volcanic centre of the Newer Cones field. However, Pb isotope data for Mt Gambier show slightly higher values (Van Otterloo *et al.*, 2014). Thus far, isotope data for the Newer Plains have been limited to $(^{87}Sr/^{86}Sr)_i$ only (Price *et al.*, 1997); these show higher isotopic ratios compared with the other series for a wide range in Mg-number (Fig. 7a). Our Newer Cones data generally show a narrower range in Sr, Nd and Pb isotope compositions compared with those of the Older Volcanics and Euroa Volcanics (Fig. 7a–d). These latter two series show more scatter than our new data but none of the series displays an obvious trend in Mg-number vs initial isotopic ratio plots (Fig. 7a–d). As observed by Price *et al.* (2014), all series overlap the mantle array in a $(^{87}Sr/^{86}Sr)_i$ vs $(^{143}Nd/^{144}Nd)_i$ isotope diagram, with the Older Volcanics defining a steeper slope (Fig. 8a). There is no obvious correlation between trace element signature and isotope variation, as the difference in Sr–Nd isotope trends for the Older Volcanics is independent of Ce/Pb and Nb/U ratio, as are the high Sr isotope ratios for the Newer Plains. Pb isotope data for our samples display a parallel trend to the NHRL that is also observed for the Older Volcanics and Euroa Volcanics (Fig. 8b and c). A $(^{207}Pb/^{204}Pb)_i$ vs $(^{143}Nd/^{144}Nd)_i$ diagram (Fig. 8d) shows that data for the Older Volcanics, Euroa Volcanics and Newer Cones trend towards mantle xenoliths of different isotopic composition (Stolz & Davies, 1988), indicative of a heterogeneous source.

Petrogenesis

Partial melting

Distinct isotope and trace element compositions differentiate the Older Volcanics from the Euroa Volcanics

Table 2: Sr–Nd–Pb isotope data for the Newer Cones

	Sr (ppm)	Nd (ppm)	Pb (ppm)	$^{87}Sr/^{86}Sr$	2σ	$^{143}Nd/^{144}Nd$	2σ	$^{206}Pb/^{204}Pb$	2σ	$^{207}Pb/^{204}Pb$	2σ	$^{208}Pb/^{204}Pb$	2σ
VIC03	1044·3	62·90	5·3	0·70387	1·59E – 05	0·51284	5·95E – 06	18·8333	2·67E – 02	15·6112	1·23E – 03	38·6758	3·13E – 02
VIC06	477·0	26·00	2·8	0·70455	1·88E – 05	0·51278	7·32E – 06	18·7927	2·54E – 02	15·6359	1·17E – 02	38·8884	2·88E – 02
VIC09	1095·6	54·70	6·7	0·70394	1·44E – 05	0·51284	6·10E – 06	18·7441	2·35E – 02	15·5909	1·08E – 03	38·7035	2·75E – 02
VIC16	529·9	24·00	2·1	0·70396	5·12E – 08	0·51283	3·91E – 08	18·5334	1·48E – 04	15·6019	6·82E – 06	38·6134	1·95E – 04
VIC17	536·5	23·00	3·4	0·70401	8·25E – 08	0·51283	4·75E – 08	18·4525	9·09E – 05	15·5472	4·19E – 06	38·4706	1·40E – 04
VIC18	69·9	25·50	2·3	0·70390	1·49E – 05	0·51283	7·09E – 06	18·5041	2·38E – 02	15·5876	1·10E – 03	38·5615	3·36E – 02
VIC21	959·0	43·20	2·8	0·70392	6·93E – 08	0·51286	3·99E – 08	18·5348	2·34E – 04	15·5952	1·08E – 05	38·5757	2·49E – 04
VIC25	876·4	46·00	4·0	0·70424	2·35E – 06	0·51281	8·45E – 07	18·6453	4·17E – 03	15·5846	1·92E – 04	38·7449	4·86E – 03
VIC29	677·8	31·40	3·1	0·70388	1·16E – 06	0·51284	9·58E – 07	18·6072	2·17E – 03	15·5706	1·00E – 04	38·6349	2·39E – 03

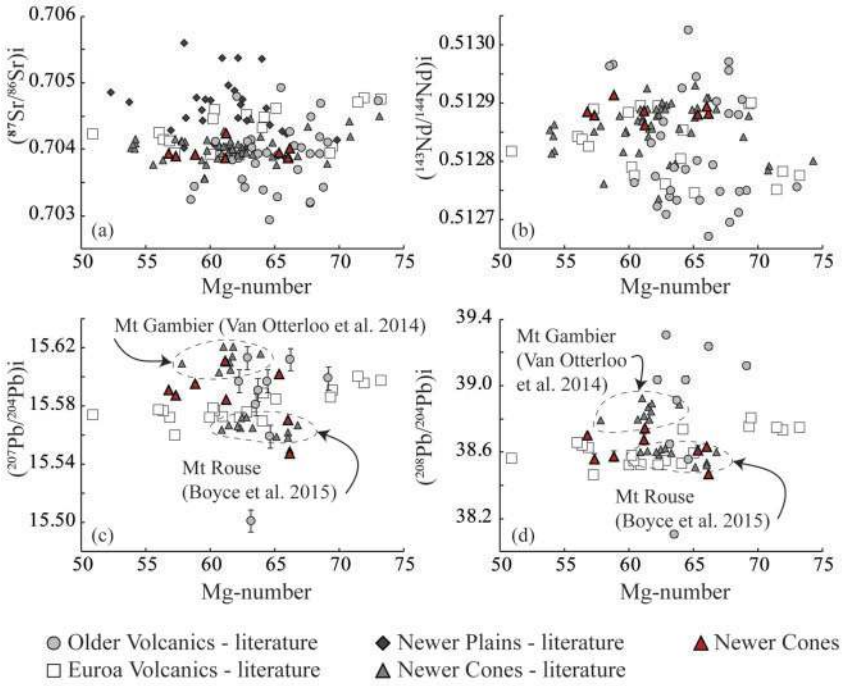

Fig. 7. $(^{87}Sr/^{86}Sr)_i$, $(^{143}Nd/^{144}Nd)_i$, $(^{207}Pb/^{204}Pb)_i$ and $(^{208}Pb/^{204}Pb)_i$ vs Mg-number [atomic ratio of 100 Mg/(Mg + 0·85 Fe_{tot})]. All isotope data are corrected to initial values; Newer Cones 500–41 ka, Newer Plains 4·6–1 Ma, Euroa Volcanics 7 Ma; Older Volcanics 95–19 Ma. Error bars (2σ) are indicated in (c), but are smaller than the symbols for the $^{87}Sr/^{86}Sr$, $^{143}Nd/^{144}Nd$ and $^{208}Pb/^{204}Pb$ isotope data. Published Pb isotope data for the Newer Cones are limited to recent studies of Mt Rouse (Boyce *et al.*, 2015) and Mt Gambier (Van Otterloo *et al.*, 2014); the respective fields are indicated in (c) and (d). No major element data are available for the basalts analysed for Pb isotope composition by Cooper & Green (1969). Other data sources are as in Fig. 2.

and the Newer Cones and Newer Plains series, as illustrated by the different trends between the series on bivariate REE ratio diagrams (Fig. 9a and b). Whereas the Euroa Volcanics and Newer Cones and Newer Plains show a narrow range in LREE/MREE $[(La/Sm)_{C1}$ of 2·5–5] and high MREE/HREE $[(Sm/Yb)_{C1}$ of 3–9·5], the Older Volcanics show a slightly wider range in LREE/MREE $[(La/Sm)_{C1}$ of 2·5–6] and lower MREE/HREE $[(Sm/Yb)_{C1}$ of 2–6] values. Trace element behaviour in all series is independent of Mg-number variations (Fig. 4) and therefore the observed trends cannot be explained by either fractional crystallization or crustal contamination processes. On the contrary, the different trends observed among the Cretaceous and Cenozoic intraplate basalts of southeastern Australia are most probably caused by subtle variations in the melting modalities of their respective sources.

To test the melting conditions we have used the standard equation from Shaw (1970), which describes trace element distribution during partial melting. The model was applied only to samples with less than 5% fractional crystallization. A wide range of published trace element concentrations for peridotite xenoliths from the NVP (Frey & Green, 1974; O'Reilly & Griffin, 1984; Yaxley *et al.*, 1997; Foden *et al.*, 2002) was used to constrain the composition of the potential initial source. We found that the trace element distribution patterns of the Newer Cones, Newer Plains and Euroa Volcanics are best represented by up to ~15% batch melting of a hydrous, garnet-bearing lherzolite source with a modal composition of 57 wt % olivine, 25 wt % orthopyroxene, 11 wt % clinopyroxene, 6 wt % amphibole and 2 wt% garnet (La 0·26 ppm, La/Yb 15, La/Sm 2). However, the Older Volcanics are better represented by smaller degrees (5–10%) of batch melting of a hydrous, spinel-bearing lherzolite source with a modal composition of 55 wt % olivine, 25 wt % orthopyroxene, 11 wt % clinopyroxene, 8 wt % amphibole and 1 wt % spinel (La 0·35 ppm, La/Yb 15, La/Sm 1; Fig. 9a and b). These results indicate that over time, the mantle source beneath SE Australia became more enriched in MREE, and that degrees of partial melting, as well as depth of melting, slightly increased. These degrees of partial melting are slightly higher than those suggested for different intraplate volcanic centres in similar settings, such as, for example, 5–7% for lava shields of the Jeju Island volcanic field, South Korea (Brenna *et al.*, 2010) and 2–3% for alkaline basalts in the Auckland Volcanic field (McGee *et al.*, 2011). It is important to note that for this modelling we have assumed that the source region is predominantly homogeneous; however, trends in isotope variation diagrams are an indication that source

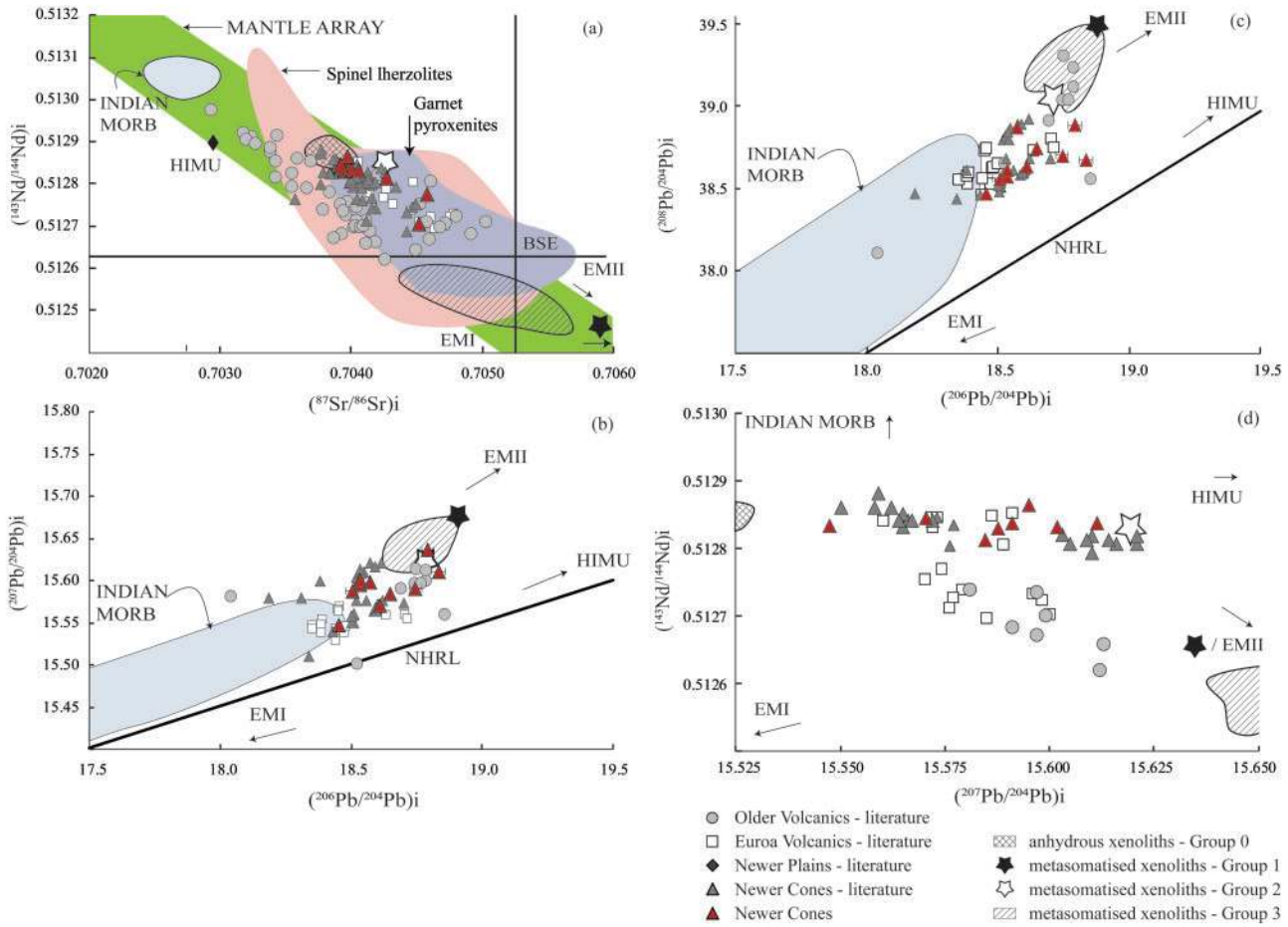

Fig. 8. (a) $(^{87}Sr/^{86}Sr)_i$ vs $(^{143}Nd/^{144}Nd)_i$, showing the mantle array in green and approximate locations of mantle end-members. Indicated are fields for Newer Volcanic Province spinel lherzolite (pink) and garnet pyroxenite (purple) xenoliths (McDonough *et al.*, 1985; Griffin *et al.*, 1988; O'Reilly & Griffin, 1988; Yaxley *et al.*, 1991; Powell *et al.*, 2004) as well as Group 0 anhydrous xenoliths (cross-hatched), Group 1 CO_2 fluid metasomatized (black star), Group 2 alkaline melt metasomatized (white star) and Group 3 carbonatite metasomatized xenoliths (diagonal lines) after Stolz & Davies (1988). (b) $(^{207}Pb/^{204}Pb)_i$ vs $(^{206}Pb/^{204}Pb)_i$ and (c) $(^{208}Pb/^{204}Pb)_i$ vs $(^{206}Pb/^{204}Pb)_i$ indicating fields for xenoliths after Stolz & Davies (1988). NHRL, Northern Hemisphere Reference Line. Newer Cones literature data are from Cooper & Green (1969), Stolz & Davies (1988), Van Otterloo *et al.* (2014) and Boyce *et al.* (2015). (d) $(^{207}Pb/^{204}Pb)_i$ vs $(^{143}Nd/^{144}Nd)_i$ showing the isotopic variation in the Older Volcanics, Euroa Volcanics and Newer Cones, as well as the isotope composition of various mantle end-members: enriched mantle I (EMI), enriched mantle II (EMII) and UIMU (High-μ; high $^{238}U/^{204}Pb$) (Stracke *et al.*, 2005), and the isotope compositions of the various groups of mantle xenoliths from Stolz & Davies (1988). Other data sources as in Fig. 2.

heterogeneity could have played an important role in the petrogenesis of the southeastern Australian intraplate basalts. Therefore, the degrees of partial melting found for all series most probably indicate maximum values.

Fractional crystallization

Covariation on major element variation diagrams as well as subparallel REE patterns on chondrite (C1) normalized REE diagrams suggest that all series might have undergone some fractional crystallization. We used the MELTS algorithm (Ghiorso & Sack, 1995) to test this hypothesis for the Newer Cones sample suite and to quantify further the extent of fractional crystallization for all series. We have used model parameters for isobaric cooling at low pressure (1 kbar) from 1200 to 800°C [fO_2 = QFM (quartz–fayalite–magnetite)] using our least differentiated sample VIC33 (MgO = 11·2 wt %; Ni = 277 ppm, Cr = 367 ppm) as starting composition. Figure 10a shows that the magmas represented by the Newer Cones basalts could have been generated by up to 20% fractional crystallization of olivine and clinopyroxene. This process led the remaining liquid to be progressively enriched in Al_2O_3. A few other Newer Cones samples previously studied have probably undergone similar amounts of fractional crystallization, but were potentially generated from a more primitive initial composition. The Older Volcanics as well as the Newer Plains show similar trends to the Newer Cones on MgO vs Al_2O_3 diagrams, and these can also be explained by up to 20% fractional crystallization using physical conditions similar to those applicable to the Newer Cones (isobaric cooling at low pressure (1 kbar) from 1200 to 800°C, fO_2 = QFM). The Euroa Volcanics show a different trend, possibly because of plagioclase crystallization in

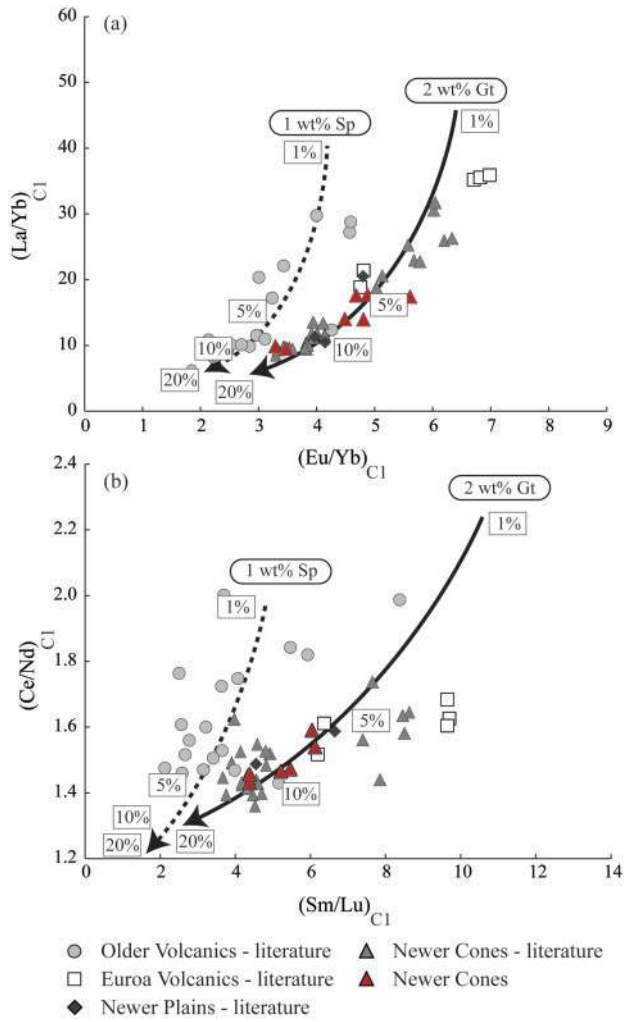

Fig. 9. Models for trace element fractionation during non-modal partial melting of Newer Volcanic Province xenolith compositions (Griffin *et al.*, 1988; Stolz & Davies, 1988; Yaxley *et al.*, 1991) with either added garnet (continuous line) or added spinel (dashed line), using the equation from Shaw (1970). Only basalt samples are plotted for which less than 5% fractional crystallization is inferred. Compositions are normalized to chondrite after Sun & McDonough (1989). Trace element distribution coefficients are from McKenzie & O'Nions (1983). Starting modal composition: continuous line: 56 wt % olivine, 25 wt % orthopyroxene, 11 wt % clinopyroxene, 2 wt % garnet, 6 wt % amphibole and La/Yb = 11; dashed line: 56 wt % olivine, 25 wt % orthopyroxene, 11 wt % clinopyroxene, 1 wt % spinel, 7 wt % amphibole and La/Yb = 15. Melting mode modified from Walter (1998): ol 0·08, opx –0·19, cpx 0·81, gt 0·15 and sp 0·15. Data sources as in Fig. 2. Numbers in rectangles indicate per cent melting.

the more evolved melts. These rocks have high MgO contents; however, olivine compositions are in good agreement with olivine that crystallizes in equilibrium with liquids having compositions similar to the bulk-rock analyses of these rocks, indicating that these rocks are unlikely to be cumulates (Paul *et al.*, 2005). MELTS modelling is compatible with these rocks being formed in a slightly more oxidizing environment (fO_2 = QFM + 2) using melting conditions similar to those applied in other cases (isobaric at 1 kbar, 1200–800°C). However, deviation from the modelled fractionation trend for some Euroa samples suggests that these results are indicative only. Paul *et al.* (2005) reported the presence of leucite in some of the most primitive samples, which could indicate derivation of the Euroa Volcanics from a more enriched mantle source, or the generation of undersaturated melts by a lower degree of melting.

Crustal contamination

The basement below South Australia and Victoria is complex in both structure and stratigraphy, containing fragments of Neoproterozoic continental crust incorporated into eastward younging Palaeozoic subduction–accretionary wedges. Furthermore, it includes Cambrian–Ordovician boninitic and MORB-type tholeiitic volcanic rocks as well as deep-ocean sedimentary rocks and arc-related volcanic rocks (Cayley *et al.*, 2011). McBride *et al.* (2001) suggested on the basis of osmium isotopes that the Newer Plains ($^{187}Os/^{188}Os$ 0·18096 ± 52 to 0·4456 ± 22) basalts might have been crustally contaminated [upper continental crust having much higher $^{187}Os/^{188}Os$ of *c.* 1·4 based on a $^{187}Re/^{188}Os$ isotope ratio of 34·4; Peucker-Ehrenbrink & Jahn (2001)], in contrast to the Newer Cones, which display $^{187}Os/^{188}Os$ ratios compatible with a derivation from an uncontaminated OIB-like mantle source ($^{187}Os/^{188}Os$ of 0·13423 ± 33 and 0·13677 ± 37). A narrow range of $(^{87}Sr/^{86}Sr)_i$ compositions over a wide range of Mg-numbers (73–54) and Ce/Pb and Nb/U ratios similar to those for OIB and MORB (Fig. 4) show that most of the Newer Cones and Euroa Volcanics are indeed unlikely to have been affected by crustal contamination. On the other hand, negative covariation between Sr isotopes and bulk-rock Sr element concentration, as well as non-OIB or MORB-like Ce/Pb and Nb/U ratios (Hofmann *et al.*, 1986) for the Older Volcanics, Newer Plains and one Newer Cones sample (VIC06), suggests that contamination by upper or lower continental crust might have affected at least some of these basalts. We have used the energy-constrained recharge, assimilation and fractional crystallization (EC-RA_xFC) algorithm (Bohrson & Spera, 2001; Spera, 2001) to investigate the possible extent of crustal assimilation in these potentially contaminated rocks. Owing to the complexity of the crust as outlined above, we have used data for average upper and lower continental crust (Taylor & McLennan, 1995) instead of detailed compositions for each structural zone. Table 3 provides the thermal and compositional input parameters used for the modelling. The Newer Cones do not show any correlation between Sr and $(^{87}Sr/^{86}Sr)_i$ other than that expected of fractional crystallization, suggesting that crustal contamination was either absent or well below 1% (Fig. 11a). The Euroa Volcanics show a similar narrow range in Sr isotope composition over a wide range of Sr concentrations. Covariation in Sr isotope composition vs Sr concentration is also absent for the Older Volcanics. However, $(^{87}Sr/^{86}Sr)_i$ values for the Newer

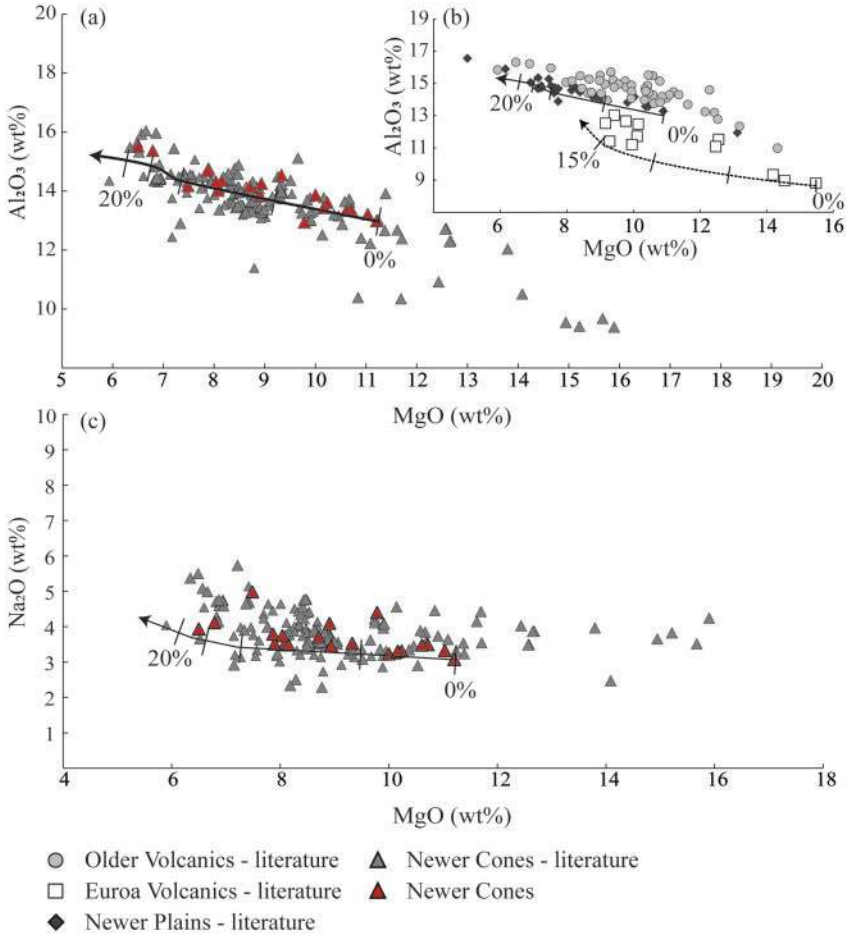

Fig. 10. MELTS (Ghiorso & Sack, 1995) modelling results for (a) and (c) the Newer Cones and (b) the Older Volcanics, Euroa Volcanics and Newer Plains. Data sources as in Fig. 2. Continuous lines represent isobaric (1 kbar) cooling (from 1200 to 800°C) of a dry magma, $fO_2 = \text{QFM} + 1$; dashed line represents isobaric (1 kbar) cooling (from 1200 to 800°C) of a dry magma, $fO_2 = \text{QFM} + 2$. Tick marks represent 5% steps.

Plains increase with decreasing Sr concentration, which can be satisfactorily modelled by up to 5% assimilation of average upper continental crust using the most primitive composition among these basalts (Fig. 11b). Whereas the majority of the Newer Plains Sr isotope compositions are suggestive of crustal assimilation, with high Sr initial ratios, most of the Older Volcanics, Euroa Volcanics and the majority of the Newer Cones appear to be uncontaminated, as noted above. Their initial Sr, Nd and Pb isotope ratios probably reflect their mantle source characteristics. Whereas a slightly low Nb/U ratio for VIC06 is suggestive of significant crustal contamination, depletion in U for VIC14 is indicative of potential fluid interaction and thus alteration; these samples are therefore omitted from the following discussion.

Mantle source compositions

Identifying potential mantle end-members

Even though agreement exists over the involvement of partial melting and open (assimilation) and closed (fractional crystallization) processes contributing to the geochemical characteristics of the basalts of the Older Volcanics, Euroa Volcanics, Newer Plains and Newer Cones, the possible contribution of the lithosphere and asthenosphere in terms of mantle sources remains contentious. Whereas some researchers favour partial melting of the asthenosphere, either of homogeneous composition (Paul *et al.*, 2005) or changing over time (Zhang *et al.*, 1999), others argue for melting of the lithospheric mantle and entrainment of this melt into the convecting asthenosphere (Price *et al.*, 1997, 2014).

The southeastern Australian lithospheric mantle has been extensively sampled by exhumed spinel lherzolite and garnet pyroxenite xenoliths, which have undergone up to three metasomatic events, as represented in the xenolith suites of many of the Newer Cones (McDonough & McCulloch, 1987; Griffin *et al.*, 1988; O'Reilly & Griffin, 1988; Stolz & Davies, 1988; Yaxley *et al.*, 1991; Powell *et al.*, 2004). On a $(^{87}Sr/^{86}Sr)_i$ vs $(^{143}Nd/^{144}Nd)_i$ isotope diagram (Fig. 8a) the Newer Cones and the Euroa Volcanics overlap the isotope compositions of SE Australian spinel lherzolites and garnet pyroxenites. Some samples of the Older Volcanics have less radiogenic $(^{87}Sr/^{86}Sr)_i$

Table 3: Input parameters for EC-RA$_x$FC modelling, thermal parameters, and standard upper and lower crustal composition after Bohrson & Spera (2001)

	Thermal parameters			
	Upper crust	Lower crust		
Magma liquidus temperature, $T_{l,m}$	1280°C	1320°C	Crystallization enthalpy, Δh_{cry} (J kg^{-1})[Q15]	396000
Magma initial temperature, T_m^0	1280°C	1320°C	Isobaric specific heat of magma, $C_{p,m}$ (J kg^{-1} K^{-1})	1484
Assimilant liquidus temperature, $T_{l,a}$	1000°C	1100°C	Fusion enthalpy, Δh_{fus} (J kg^{-1})	270000
Assimilant initial temperature, T_a^0	300°C	600°C	Isobaric specific heat of assimilant, $C_{p,a}$ (J kg^{-1} K^{-1})	1370
Solidus temperature, T_s	900°C	950°C		
Equilibrium temperature, T_{eq}	980°C	980°C		

	Compositional parameters			
	Newer Cones		Newer Plains	
	Upper crust Sr	Lower crust Sr	Upper crust Sr	Lower crust Sr
Magma initial concentration (ppm), C_m^0	1095·6	1095·6	718	718
Magma isotope ratio, ε_m	0·70394	0·70394	0·70415	0·70415
Magma trace element distribution coefficient, D_m	1·5	1·5	1·5	1·5
Enthalpy of trace element distribution reaction, ΔH_m	—	—	—	—
Assimilant initial concentration (ppm), C_a^0	350	230	350	230
Assimilant isotope ratio, ε_a	0·722	0·7100	0·722	0·7100
Assimilant trace element distribution coefficient, D_a	1·5	0·05	1·5	0·05
Enthalpy of trace element distribution reaction, ΔH_a	—		—	—

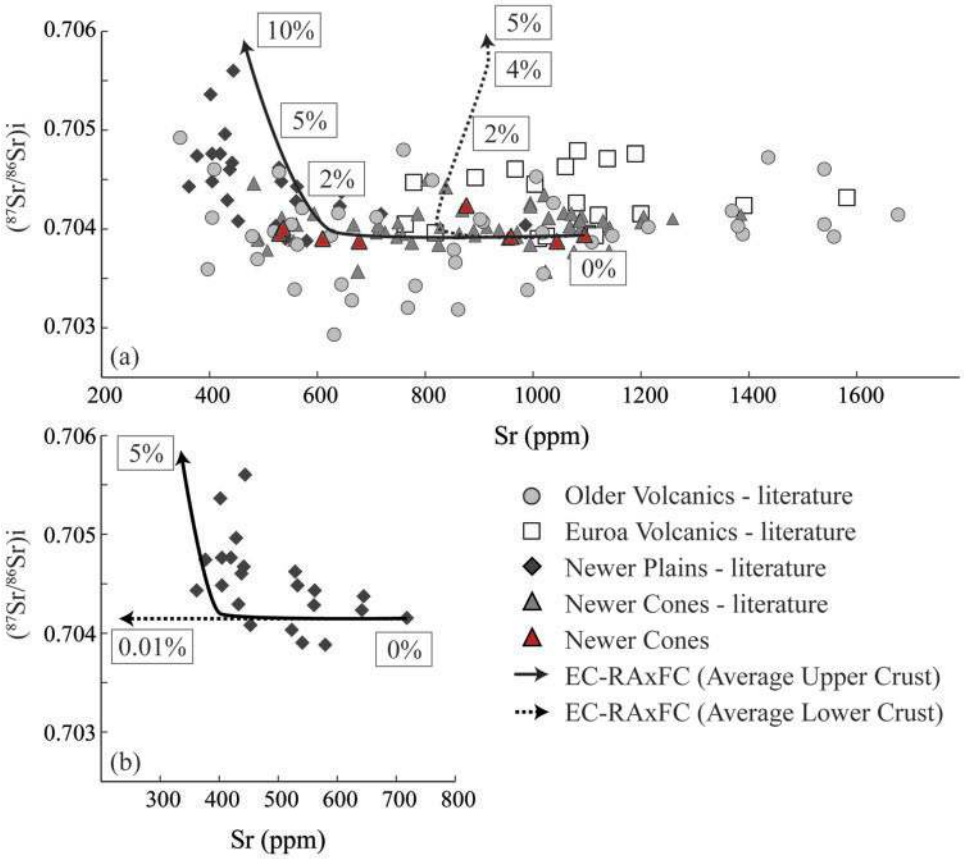

Fig. 11. (a) Sr (ppm) vs ^{87}Sr/^{86}Sr for all Newer Cones samples showing EC-RA$_x$FC modelling using input parameters as in Table 3. (b) Enlarged section of (a) showing EC-RA$_x$FC modelling results for the Newer Plains (Price *et al.*, 1997, 2014) using input parameters as in Table 3. The continuous and dashed lines represent assimilation and fractional crystallization of average upper and lower crust (Taylor & McLennan, 1995), respectively.

compositions trending toward Indian MORB compositions (Fig. 8a). This suggests that a mantle source such as Indian MORB-source asthenosphere may be considered as one of the end-members for these rocks, which is in agreement with our trace element modelling.

As far as we are aware, only Stolz & Davies (1988) have presented Pb isotope data for the xenoliths of the NVP; these have heterogeneous Pb isotope compositions, which are representative of the lithospheric mantle beneath the region. Stolz & Davies subdivided spinel lherzolites from Mount Gnotuk and Lake Bullenmerri into four suites based on their trace element and isotope compositions: Group 0: depleted, anhydrous xenoliths with Pb isotope composition similar to isotopically distinct Indian MORB (Rehkamper & Hofmann, 1997); Group 1: enriched, anhydrous xenoliths, probably metasomatized by CO_2-rich fluids, with Pb isotope compositions trending towards EMII; Group 2: hydrous xenoliths probably metasomatized by interaction between alkaline magmas and the source of the depleted anhydrous xenoliths (Group 0) with Pb isotope compositions similar to Group 3, but having lower Sr isotope and higher Nd isotope compositions respectively; Group 3: hydrous xenoliths metasomatized subsequently by fluids originating from deeper levels in the mantle with Pb isotope composition similar to Group 2, but having higher Sr isotope and lower Nd isotope compositions (Stolz & Davies, 1988). The metasomatic agent for this last group is suspected to be calcio-carbonatite fluid (Stolz & Davies, 1988); the Sr–Nd isotope compositions of this group overlap with those of Group B of Powell *et al.* (2004), which are interpreted to have undergone carbonatite metasomatism. Price *et al.* (2014) also indicated the potential for 1% calcio-carbonatite fluid to have been added to depleted mantle to generate the range of Older Volcanics with distinctive negative K anomalies.

The difference between the three basalt groups is expressed in a $(^{207}Pb/^{204}Pb)_i$ vs $(^{143}Nd/^{144}Nd)_i$ diagram, where there is a clear distinction between the trends of the Newer Cones, Euroa Volcanics and Older Volcanics (Fig. 12). As a consequence, we propose that the isotopic compositions of the Older Volcanics and part of the Euroa Volcanics can be explained by binary mixing between a mantle source similar to the depleted asthenospheric source of Indian MORB and metasomatized lithospheric mantle represented by the Group 3 xenoliths. In contrast, the isotopic signature of the Newer Cones is more consistent with binary mixing between mantle sources similar to the Group 0 and Group 2 xenoliths. We modelled this mixing using the equation of Vollmer (1976).

Figure 12a (blue lines) shows that the range of Older Volcanics isotope compositions can be generated by mixing of Indian MORB-source mantle ($^{143}Nd/^{144}Nd = 0{\cdot}51303$, $^{207}Pb/^{204}Pb = 15{\cdot}486$ [based on the average composition of Indian MORB reported by Stracke *et al.* (2003)], [Nd] = 9 ppm and [Pb] = 0·6 ppm (Sun & McDonough, 1989) and a small-degree partial melt derived from the protolith of the Group 3 xenoliths ($^{143}Nd/^{144}Nd = 0{\cdot}512523$, $^{207}Pb/^{204}Pb = 15{\cdot}6424$; Stolz & Davies, 1988). Trace element concentrations used for mixing modelling of the Group 3 xenoliths were [Nd] = 167·78 ppm and [Pb] = 13·68 ppm and Nd = 85·24 ppm and Pb = 3·17 ppm derived from calculations based on 1% and 5% batch melting, respectively, of the most primitive Group 3 xenolith (MgO = 41·02 wt %, [Ni] = 2072 ppm, [Cr] = 5967 ppm; Stolz & Davies, 1988). It is shown that the Older Volcanics with low $^{143}Nd/^{144}Nd$ for a given $^{207}Pb/^{204}Pb$ can be derived from a source comprising Indian MORB-source mantle to which 5–10% of small-degree Group 3 melts are added (1% partial melting of the original peridotite), whereas the Older Volcanics with slightly higher $^{143}Nd/^{144}Nd$ for a given $^{207}Pb/^{204}Pb$ are more probably derived from a source resulting from mixing of Indian MORB-source mantle and up to 40% Group 3 melt (5% partial melting). The Group 0 depleted, anhydrous xenoliths of Stolz & Davies (1988) have Pb isotope compositions similar to Indian MORB, but have slightly higher and lower Sr and Nd isotope compositions, respectively. We propose that subsequent interaction of Indian MORB-source mantle with the alkaline melts that generated the Older Volcanics could have generated the protolith of the Group 0 xenoliths. Mixing between the most primitive of the Older Volcanics [$(^{143}Nd/^{144}Nd)_i = 0{\cdot}5127$, $(^{207}Pb/^{204}Pb)_i = 15{\cdot}599$, Mg-number = 69 (Price *et al.*, 2014)] and Indian MORB-source mantle, with the composition given above, shows that adding *c.* 10% alkaline melt to Indian MORB-source mantle lowers the Nd isotope composition towards that of the Group 0 xenoliths (Fig. 12b, green line).

The Newer Cones, however, show contrasting behaviour with a very narrow range in Nd isotope composition for a given $(^{207}Pb/^{204}Pb)_i$, forming a trend between the Group 0 and Group 2 xenoliths. Mixing between Group 0 ($^{143}Nd/^{144}Nd = 0{\cdot}51285$, $^{207}Pb/^{204}Pb = 15{\cdot}507$, [Nd] = 1·36 ppm and [Pb] = 0·019 ppm) and Group 2 ($^{143}Nd/^{144}Nd = 0{\cdot}512841$, $^{207}Pb/^{204}Pb = 15{\cdot}619$, [Nd] = 4·86 ppm and [Pb] = 0·059 ppm; Stolz & Davies, 1988) sources shows that VIC17 can be generated by only 10% addition of Group 2 into the depleted anhydrous mantle, whereas VIC03 requires a greater amount of mixing (~80% of Group 2; Fig. 12c). There is no direct evidence that carbonatite metasomatized xenoliths (Group 3) have had much influence in the generation of the Newer Cones basalts.

The Euroa Volcanics are divided into two groups of which the majority approximately follow the trend of the Older Volcanics (Fig. 12a), whereas the data for samples from Seven Creeks West (Paul *et al.*, 2005) overlap with our data on the Newer Cones (Fig. 12c). It would be interesting to determine the age of the samples from the Seven Creeks, as an old age would imply that they originated from the same process as the Older Volcanics, as described above, whereas ages similar to the Newer Cones would indicate that they were derived by melting of mixed Group 0 and Group 2 lithospheric mantle sources.

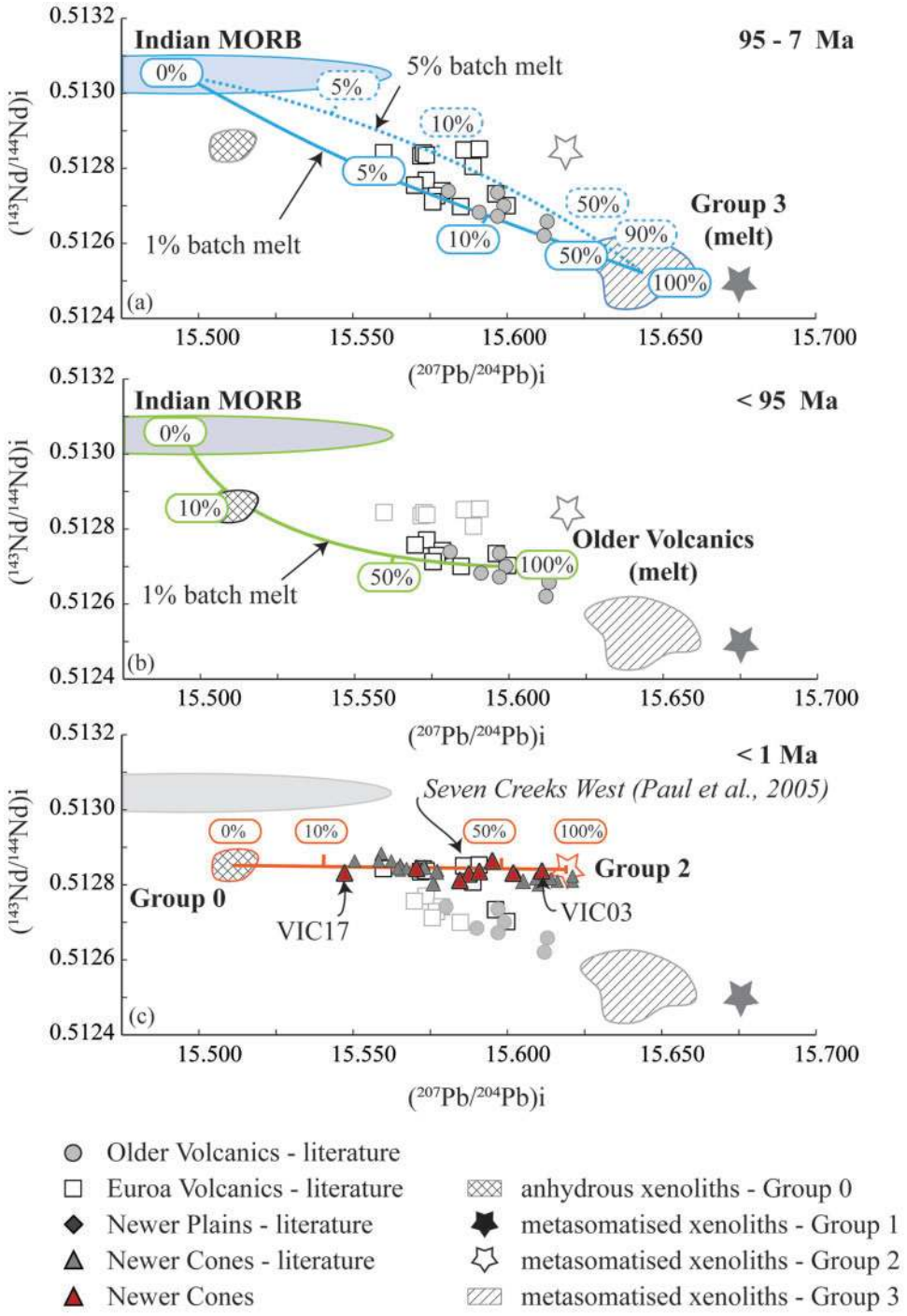

Fig. 12. $(^{207}Pb/^{204}Pb)_i$ vs $(^{143}Nd/^{144}Nd)_i$ for samples interpreted to represent magmas unaffected by crustal assimilation showing: (a) calculated mixing line (Vollmer, 1976) between Indian MORB-source mantle and melts derived by 1% (blue continuous line) and 5% (blue dashed line) partial melting of Group 3 xenoliths; (b) calculated mixing line between Indian MORB-source mantle and the most primitive sample (Mg-number = 67) of the Older Volcanics (green continuous line); (c) calculated mixing line between Group 0 and Group 2 xenoliths. It should be noted that the Euroa Volcanics plot in two groups. The Seven Creek West samples (Paul *et al.*, 2005) are indicated.

In summary, whereas the 95–19 Ma Older Volcanics as well as part of the Euroa Volcanics have isotopic compositions indicating basalt generation from a source with isotope characteristics similar to that of a mixture between Indian MORB-source mantle and small-degree partial melts of the protolith of Group 3 (carbonatite metasomatized) xenoliths, the <1 Ma Newer Plains and perhaps the remainder of the Euroa

Volcanics show that basalt generation can be explained entirely by melting of a distinctively different suite of source materials comprising modified Indian MORB-source mantle (Group 0) and alkaline melt metasomatized xenoliths (Group 2). Our model compares well with, and is an extension of, the model of Price *et al.* (2014), who suggested mixing of 1% calcio-carbonatite fluid to the depleted mantle to generate the geochemical signature of the Older Volcanics.

Geodynamics

A recent teleseismic tomography study (Davies & Rawlinson, 2014), based on variations in P-wave velocity, has revealed the presence of a low-velocity anomaly in the upper mantle that spatially corresponds to the surface extent of the NVP. Such an anomaly is indicative of the presence of elevated temperatures (mantle plume) and/or a region of partial melt in the upper mantle (Davies & Rawlinson, 2014), the latter hypothesis being preferred owing to the limited topographic response in the region (Demidjuk *et al.*, 2007). The existence of U/Th disequilibria showing a ^{230}Th excess of 12–57% (Demidjuk *et al.*, 2007) is suggestive of dynamic melting in the upwelling upper asthenosphere rather than static batch melting within the lithosphere, an interpretation that is supported by magnetotelluric sounding that provides evidence for decompression melting in the upper asthenosphere (Aivazpourporgou *et al.*, 2015). It is thought that this upwelling is triggered by three-dimensional (3D) thickness variations in the lithosphere causing edge-driven convection (King & Anderson, 1998). Rapid plate movement from 40 Ma onwards, after the separation of Antarctica and Australia (Veevers, 1986), resulted in a fast, northward plate movement of 6·5 cm a^{-1} (Sella *et al.*, 2002). As this plate movement is perpendicular to a step in lithospheric thickness (Demidjuk *et al.*, 2007) and plate movement is $>$1 cm a^{-1}, edge-driven convection with shear resulting in upwelling is postulated to be the geodynamic cause of the NVP magmatism (Conrad *et al.*, 2011). Convection cell sizes of the order of 150–200 km may form during edge-driven convection (King & Anderson, 1998), which is comparable with the spatial extent of volcanism in SE Australia. Recent edge-driven convection modelling for the Moroccan Cenozoic volcanic province (Kaislaniemi & Van Hunen, 2014) shows that upwelling mantle (1) facilitates decompression melting, removing any hydrous mantle components, and (2) erodes the bottom of the mantle lithosphere, entraining the residual depleted lithosphere. Furthermore, that study found that edge-driven convection with shear produces convection rolls with axes perpendicular to lithosphere thickness steps. The complex lithosphere configuration beneath Victoria, with a stacked alternation of continental (Delamerian) and continental and oceanic (Lachlan) crust, as well as a locally constrained continental section of the Selwyn block within the Lachlan fold belt, potentially generates a complex 3D configuration of convection rolls, capable of variably focusing the loci of upwelling and associated magmatism in the region.

Figure 13a shows a schematic representation of our interpretation of the processes leading to the genesis of the Older Volcanics, Euroa Volcanics, Newer Plains and Newer Cones magmatism. Using the different xenolith groups as proxies for larger scale mantle components [Group 0 = modified Indian MORB-source mantle ('MORB-B'); Group 2 = depleted SCLM; Group 1 and Group 3 = veined SCLM] we can deduce the spatial and temporal variations in the composition of the mantle beneath SE Australia. We suggest that at the time of earliest basalt generation (Fig. 13b) the mantle beneath Victoria consisted of an Indian MORB-source asthenosphere (MORB-A) and a veined, Group 3-type SCLM (O'Reilly & Griffin, 1988). Such veins can have solidus temperatures up to 200°C lower than their surrounding wall-rocks (Foden *et al.*, 2002) and will melt first during decompression melting at the base of the lithosphere. Mixing of melts of these veins with upwelling Indian MORB-source mantle potentially resulted in the distinct $(Sm/Yb)_{C1}$, $(Eu/Yb)_{C1}$ and Pb and Nd isotope signatures of the Older Volcanics and part of the Euroa Volcanics. Prolonged periods of decompression melting could have caused minor modification of the Indian MORB-source asthenosphere (MORB-B) owing to mixing of alkaline melts with this source as evidenced by the Group 0 xenolith compositions (Stolz & Davies, 1988; Figs 12b and 13c). Furthermore, continuing vein melting in the region of decompression melting would have purged the SCLM of enriched Group 3 veins, leaving a more depleted residual SCLM (Fig. 13d). As upwelling continued (Fig. 13e), thermal erosion of the depleted residual SCLM potentially resulted in lithosphere delamination and mixing of this depleted SCLM with modified Indian MORB-source asthenosphere; which in turn was the source of the basalts of the Newer Plains and Newer Cones. High degrees of partial melting following lithosphere delamination could have resulted in the volumetrically dominant, tholeiitic Newer Plains magmas. As the Newer Plains magmatic rocks are relatively depleted in incompatible elements compared with the Newer Cones, crustal contamination would have affected their isotope and trace element compositions more than the compositions of the Newer Cones. Both of these slightly deeper melts might have incorporated shallow, enriched, metasomatized xenoliths of all groups that were unaffected by decompression melting *en route* to the surface, as indicated by the presence of abundant, compositionally variable mantle xenoliths within the Newer Cones. Such a model is in agreement with recent geophysical observations in the province as well as with the wide range of pressures calculated for both Older Volcanics and Newer Cones basalt generation (1·5–4·5 GPa; Price *et al.*, 2014).

CONCLUSIONS

New major and trace element and Sr, Nd and Pb isotope data for the youngest expression of Cretaceous to

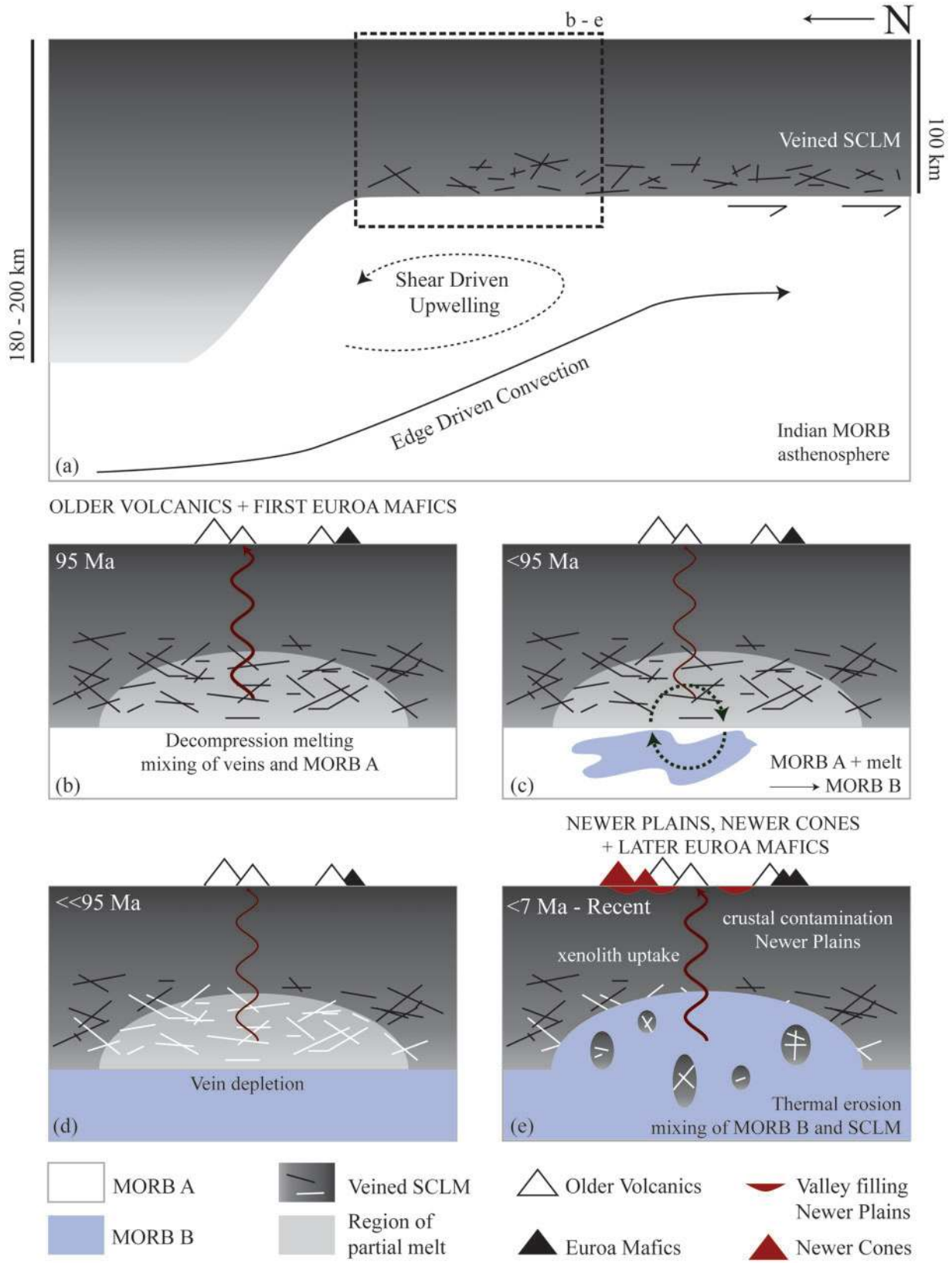

Fig. 13. (a) Interpreted temporal geodynamic evolution of the mantle below SE Australia (after Kaislaniemi & Van Hunen, 2014). Thickness to the base of the lithosphere after Davies & Rawlinson (2014). (b) Enlarged section. Decompression melting at the base of the lithosphere results in preferential melting of metasomatized veins and mixing of the resultant enriched partial melts with Indian MORB-source mantle (MORB-A) thereby generating the magmas parental to the Older Volcanics. (c) Mixing of MORB-A with the alkaline melts represented by the Older Volcanics results in a slightly modified Indian MORB-source mantle (MORB-B). (d) Prolonged periods of melting will deplete the SCLM of calcio-carbonatite metasomatized veins. (e) Continued edge-driven convection with shear causes thermal erosion of the base of the lithosphere, incorporating depleted SCLM within MORB-B. The resultant melts have the potential to incorporate enriched vein material from the SCLM *en route* to the surface.

Cenozoic volcanism in SE Australia suggest spatial and long-term temporal geochemical and geodynamic variations within the mantle below. We find that basalts of the <1 Ma Newer Cones were generated by *c.* 5–10% partial melting of a garnet–spinel mantle source, the composition of which can be represented as a mixture of depleted, anhydrous, Indian MORB-source spinel lherzolite and enriched, hydrous spinel lherzolite metasomatized by alkaline melts. The resulting melts evolved by fractional crystallization. According to our modelling, up to 20% crystallization is required to reach the composition of the analysed samples. EC-RA$_x$FC modelling shows that the Newer Cones magmas were not affected by crustal assimilation processes. Conversely, the enriched trace element and isotope signatures of the <4·6 Ma Newer Plains magmatic rocks can be modelled by up to 5% assimilation of average upper crust. The ~7 Ma Euroa Volcanics represent basaltic magmas generated by similar degrees of partial melting (10%) but slightly smaller amounts of fractional crystallization (15%). Their Pb and Nd isotope compositions suggest a heterogeneous source, which we interpret to reflect a progressive temporal change from the source of the Older Volcanics to the source of the Newer Cones. The 95–19 Ma Older Volcanics have trace element and Sr–Nd–Pb isotope signatures that are distinct from those of the other series; their source can be modelled by adding *c.* 10% melt derived by small degrees of partial melting of carbonatite metasomatized vein material to a composition similar to that of Indian MORB-source mantle. We suggest that the temporal variation in the mantle source can be explained by a geodynamical model of edge-driven convection with shear. The primary magmas of the Older Volcanics were formed by decompression melting that favoured the partial melting of hydrous, carbonatite metasomatized mantle veins. Subsequent thermal erosion and entrainment of the depleted SCLM in the locally slightly enriched upper asthenosphere resulted in the generation of the Euroa Volcanics, Newer Plains and Newer Cones.

ACKNOWLEDGEMENTS

Professor David Phillips and Dr Erin Matchan of the University of Melbourne and David Taylor of the Geological Survey of Victoria are thanked for their assistance in the field. Michèle Senn (University of Geneva) is thanked for performing the column chemistry for the Sr, Nd and Pb isotope analyses. Richard Price (University of Waikato), Lucy McGee (Universidad de Chile) and an anonymous reviewer provided constructive reviews, and Richard Price and Marjorie Wilson are thanked for editorial handling. The support of TiGER and the Department of Applied Geology at Curtin University of Technology is gratefully acknowledged.

FUNDING

This research was funded by Australian Research Council Discovery grant DP130100517.

SUPPLEMENTARY DATA

Supplementary data for this paper are available at *Journal of Petrology* online.

REFERENCES

Aivazpourporgou, S., Thiel, S., Hayman, P. C., Moresi, L. N. & Heinson, G. (2015). Decompression melting driving intraplate volcanism in Australia: Evidence from magnetotelluric sounding. *Geophysical Research Letters* **42**, 1–9.

Aziz-ur-Rahman & McDougall, I. (1972). Potassium–argon ages on the Newer Volcanics of Victoria. *Proceedings of the Royal Society of Victoria* **85**, 61–69.

Baker, J., Peate, D., Waight, T. & Meyzen, C. (2004). Pb isotopic analysis of standards and samples using a ^{207}Pb–^{204}Pb double spike and thallium to correct for mass bias with a double-focusing MC-ICPMS. *Chemical Geology* **211**, 275–303.

Blackburn, G., Allison, G. B. & Leaney, F. W. J. (1982). Further evidence on the age of tuff at Mt Gambier, South Australia. *Transactions of the Royal Society of South Australia* **106**, 163–167.

Bohrson, W. A. & Spera, F. J. (2001). Energy-constrained open-system magmatic processes II: Application of energy-constrained assimilation–fractional crystallization (EC-AFC) model to magmatic systems. *Journal of Petrology* **42**, 1019–1041.

Boyce, J. (2013). The Newer Volcanics Province of southeastern Australia: a new classification scheme and distribution map for eruption centres. *Australian Journal of Earth Sciences* **60**, 449–462.

Boyce, J. A., Nicholls, I. A., Keays, R. R. & Hayman, P. C. (2015). Composition and volatile contents of parental magmas of Mt. Rouse, a polymagmatic volcano in the Newer Volcanics intraplate basaltic province, SE Australia. *Contributions to Mineralogy and Petrology* **169**, 1–21.

Brenna, M., Cronin, S. J., Smith, I. E. M., Sohn, Y. K. & Németh, K. (2010). Mechanisms driving polymagmatic activity at a monogenetic volcano, Udo, Jeju Island, South Korea. *Contributions to Mineralogy and Petrology* **160**, 931–950.

Cartwright, I., Weaver, T., Tweed, S., Ahearne, D., Cooper, M., Czapnik, K. & Tranter, J. (2002). Stable isotope geochemistry of cold CO_2-bearing mineral spring waters, Daylesford, Victoria, Australia: Sources of gas and water and links with waning volcanism. *Chemical Geology* **185**, 71–91.

Cayley, R. A., Korsch, K. J., Moore, D. H. et al. (2011). Crustal architecture of central Victoria: results from the 2006 deep crustal reflection seismic survey. *Australian Journal of Earth Sciences* **58**, 113–156.

Chiaradia, M., Muntener, O. & Beate, B. (2011). Enriched basaltic andesites from mid-crustal fractional crystallization, recharge, and assimilation (Pilavo Volcano, Western Cordillera of Ecuador). *Journal of Petrology* **52**, 1107–1141.

Conrad, C. P., Bianco, T. A., Smith, E. I. & Wessel, P. (2011). Patterns of intraplate volcanism controlled by asthenospheric shear. *Nature Geoscience* **4**, 317–321.

Cooper, J. A. & Green, D. H. (1969). Lead isotope measurements on lherzolite inclusions and host basanites from Western Victoria, Australia. *Earth and Planetary Science Letters* **6**, 69–76.

Davies, D. R. & Rawlinson, N. (2014). On the origin of recent intraplate volcanism in Australia. *Geology* **42**, 1–4.

Davies, D. R., Rawlinson, N., Iaffaldano, G. & Campbell, I. H. (2015). Lithospheric controls on magma composition along Earth's longest continental hotspot track. *Nature* **525**, 511–514.

Day, R. A. (1983). Petrology and geochemistry of the Older Volcanics, Victoria: distribution, characterization, and petrogenesis. Monash University, PhD thesis, Department of Earth Sciences.

Day, R. A. (1989). East Australian volcanic geology; Victoria and South Australia. In: Johnson, R. W. (ed.) *Intraplate Volcanism of Eastern Australia and New Zealand*. Australian Academy of Science, pp. 132–142.

Demidjuk, Z., Turner, S., Sandiford, M., George, R., Foden, J. & Etheridge, M. (2007). U-series isotope and geodynamic constraints on mantle melting processes beneath the Newer Volcanic Province in South Australia. *Earth and Planetary Science Letters* **261**, 517–533.

Ellis, D. J. (1976). High pressure cognate inclusions in the Newer Volcanics of Victoria. *Contributions to Mineralogy and Petrology* **58**, 149–180.

Ewart, A. (2004). Petrology and geochemistry of Early Cretaceous bimodal continental flood volcanism of the NW Etendeka, Namibia. Part 1: Introduction, mafic lavas and re-evaluation of mantle source components. *Journal of Petrology* **45**, 59–105.

Foden, J., Song, S. H., Turner, S., Elburg, M., Smith, P. B., Van der Steldt, B. & Van Penglis, D. (2002). Geochemical evolution of lithospheric mantle beneath S.E. South Australia. *Chemical Geology* **182**, 663–696.

Frey, F. A. & Green, D. H. (1974). The mineralogy, geochemistry and origin of lherzolite inclusions in Victorian basanites. *Geochimica et Cosmochimica Acta* **38**, 1023–1059.

Frey, F. A., Green, D. H. & Roy, S. D. (1978). Integrated models of basalt petrogenesis: a study of quartz tholeiites to olivine melilitites from south eastern Australia utilizing geochemical and experimental petrological data. *Journal of Petrology* **19**, 463–513.

Ghiorso, M. S. & Sack, R. O. (1995). Chemical mass transfer in magmatic processes IV. A revised and internally consistent thermodynamic model for the interpolation and extrapolation of liquid–solid equilibria in magmatic systems at elevated temperatures and pressures. *Contributions to Mineralogy and Petrology* **119**, 197–212.

Gray, C. M. & McDougall, I. (2009). K–Ar geochronology of basalt petrogenesis, Newer Volcanic Province, Victoria. *Australian Journal of Earth Sciences* **56**, 245–258.

Griffin, W. L., O'Reilly, S. Y. & Stabel, A. (1988). Mantle metasomatism beneath western Victoria, Australia: II. Isotopic geochemistry. *Geochimica et Cosmochimica Acta* **52**, 449–459.

Handler, M. R., Bennett, V. C. & Esat, T. M. (1997). The persistence of off-cratonic lithospheric mantle: Os isotopic systematics of variably metasomatised southeast Australian xenoliths. *Earth and Planetary Science Letters* **151**, 61–75.

Hofmann, A. W., Jochum, K. P., Seufert, M. & White, W. M. (1986). Nb and Pb in oceanic basalts: new constraints on mantle evolution. *Earth and Planetary Science Letters* **79**, 33–45.

Irvine, T. N. & Baragar, W. R. A. (1971). A guide to the chemical classification of the common volcanic rocks. *Canadian Journal of Earth Sciences* **8**, 523–548.

Kaislaniemi, L. & Van Hunen, J. (2014). Dynamics of lithosphere thinning and mantle melting by edge-driven convection; application to the Moroccan Atlas mountains. *Geochemistry, Geophysics, Geosystems* **15**, 3175–3189.

King, S. D. & Anderson, D. L. (1998). Edge-driven convection. *Earth and Planetary Science Letters* **160**, 289–296.

Le Bas, M. J., Le Maitre, R. W., Streckeisen, A. & Zanettin, B. (1986). A chemical classification of volcanic rocks based on the total alkali vs. silica diagram. *Journal of Petrology* **27**, 745–750.

Matchan, E. L. & Phillips, D. (2011). New $^{40}Ar/^{39}Ar$ ages for selected young (<1 Ma) basalt flows of the Newer Volcanic Province, southeastern Australia. *Quaternary Geochronology* **6**, 356–368.

Matchan, E. L. & Phillips, D. (2014). High precision multi-collector $^{40}Ar/^{39}Ar$ dating of young basalts: Mount Rouse volcano (SE Australia) revisited. *Quaternary Geochronology* **22**, 57–64.

McBride, J. S., Lambert, D. D., Nicholls, I. A. & Price, R. C. (2001). Osmium isotopic evidence for crust–mantle interaction in the genesis of continental intraplate basalts from the Newer Volcanics Province, southeastern Australia. *Journal of Petrology* **42**, 1197–1218.

McDonough, W. F. & McCulloch, M. T. (1987). The southeast Australian lithospheric mantle: isotopic and geochemical constraints on its growth and evolution. *Earth and Planetary Science Letters* **86**, 327–340.

McDonough, W. F., McCulloch, M. T. & Sun, S. S. (1985). Isotopic and geochemical systematics in Tertiary–Recent basalts from southeastern Australia and implications for the evolution of the sub-continental lithosphere. *Geochimica et Cosmochimica Acta* **49**, 2051–2067.

McDougall, I., Allsopp, H. L. & Chamalaun, F. H. (1966). Isotopic dating of the newer volcanics of Victoria, Australia, and geomagnetic polarity epochs. *Journal of Geophysical Research* **71**, 6107–6118.

McGee, L. E., Beier, C., Smith, I. E. M. & Turner, S. P. (2011). Dynamics of melting beneath a small-scale basaltic system: A U–Th–Ra study from Rangitoto volcano, Auckland volcanic field, New Zealand. *Contributions to Mineralogy and Petrology* **162**, 547–563.

McGee, L. E., Smith, I. E. M., Millet, M. A., Handley, H. K. & Lindsay, J. M. (2013). Asthenospheric control of melting processes in a monogenetic basaltic system: A case study of the Auckland volcanic field, New Zealand. *Journal of Petrology* **54**, 2125–2153.

McKenzie, D. & O'Nions, R. K. (1983). Mantle reservoirs and ocean island basalts. *Nature* **301**, 229–231.

Nelson, D. R., McCulloch, M. T. & Sun, S. S. (1986). The origins of ultrapotassic rocks as inferred from Sr, Nd and Pb isotopes. *Geochimica et Cosmochimica Acta* **50**, 231–245.

Oostingh, K. F., Jourdan, F., Phillips, D. & Matchan, E. L. (2015). Ultra-precise $^{40}Ar/^{39}Ar$ geochronology and ^{38}Ar exposure dating on young basalts from the Newer Volcanic Province, Australia. *Goldschmidt 2015 Conference Abstracts* Goldschmidt Conference Abstracts, 2351.

O'Reilly, S. Y. & Griffin, W. L. (1984). Sr isotopic heterogeneity in primitive basaltic rocks, southeastern Australia: correlation with mantle metasomatism. *Contributions to Mineralogy and Petrology* **87**, 220–230.

O'Reilly, S. Y. & Griffin, W. L. (1988). Mantle metasomatism beneath western Victoria, Australia: I. Metasomatic processes in Cr-diopside lherzolites. *Geochimica et Cosmochimica Acta* **52**, 433–447.

O'Reilly, S. Y. & Zhang, M. (1995). Geochemical characteristics of lava-field basalts from eastern Australia and inferred sources: connections with the subcontinental lithospheric mantle?. *Contributions to Mineralogy and Petrology* **121**, 148–170.

Paul, B., Hergt, J. M. & Woodhead, J. D. (2005). Mantle heterogeneity beneath the Cenozoic volcanic provinces of central Victoria inferred from trace-element and Sr, Nd, Pb and Hf isotope data. *Australian Journal of Earth Sciences* **52**, 243–260.

Peucker-Ehrenbrink, B. & Jahn, B. (2001). Rhenium–osmium isotope systematics and platinum group element concentrations: Loess and the upper continental crust. *Geochemistry, Geophysics, Geosystems* **2**. DOI: 10.1029/2001GC000172.

Powell, W., Zhang, M., O'Reilly, S. Y. & Tiepolo, M. (2004). Mantle amphibole trace-element and isotopic signatures trace multiple metasomatic episodes in lithospheric mantle, western Victoria, Australia. *Lithos* **75**, 141–171.

Price, R. C., Gray, C. M. & Frey, F. A. (1997). Strontium isotopic and trace element heterogeneity in the plains basalts of the Newer Volcanic Province, Victoria, Australia. *Geochimica et Cosmochimica Acta* **61**, 171–192.

Price, R. C., Nicholls, I. A. & Gray, C. M. (2003). Cainozoic igneous activity. In: Birch, W. D. (ed.) *Geology of Victoria*. Geological Society of Australia Special Publication 23. Geological Society of Australia (Victoria Division), pp. 361–375.

Price, R. C., Nicholls, I. A. & Day, A. (2014). Lithospheric influences on magma compositions of late Mesozoic and Cenozoic intraplate basalts (the Older Volcanics) of Victoria, south-eastern Australia. *Lithos* **206–207**, 179–200.

Rehkamper, M. & Hofmann, A. W. (1997). Recycled ocean crust and sediment in Indian Ocean MORB. *Earth and Planetary Science Letters* **147**, 93–106.

Sella, G. F., Dixon, T. H. & Mao, A. (2002). REVEL: A model for Recent plate velocities from space geodesy. *Journal of Geophysical Research* **107**. DOI: 10.1029/2000JB000033.

Shaw, D. M. (1970). Trace element fractionation during anatexis. *Geochimica et Cosmochimica Acta* **34**, 237–243.

Spera, F. J. (2001). Energy-constrained open-system magmatic processes I: General model and energy-constrained assimilation and fractional crystallization (EC-AFC) formulation. *Journal of Petrology* **42**, 999–1018.

Stolz, A. J. & Davies, G. R. (1988). Chemical and isotopic evidence from spinel lherzolite xenoliths for episodic metasomatism of the upper mantle beneath southeastern Australia. *Journal of Petrology, Special Volume*, 303–330.

Stracke, A., Bizimis, M. & Salters, V. J. M. (2003). Recycling oceanic crust: Quantitative constraints. *Geochemistry, Geophysics, Geosystems* **4**. DOI: 10.1029/2001GC000223.

Stracke, A., Hofmann, A. W. & Hart, S. R. (2005). FOZO, HIMU, and the rest of the mantle zoo. *Geochemistry, Geophysics, Geosystems* **6**. DOI: 10.1029/2004GC000824.

Sun, S. S. & McDonough, W. F. (1989). Chemical and isotopic systematics of oceanic basalts: implications for mantle composition and processes. In: Saunders, A. D. & Norry, M. J. (eds) *Magmatism in the Ocean Basins. Geological Society, London, Special Publications* **42**, 313–345.

Tanaka, T., Togashi, S., Kamioka, H., Amakawa, H., Kagami, H. & Hamamoto, T. (2000). JNdi-1: a neodymium isotopic reference in consistency with LaJolla neodymium. *Chemical Geology* **168**, 279–281.

Taylor, S. R. & McLennan, S. M. (1995). The geochemical evolution of the continental crust. *Reviews of Geophysics* **33**, 241–265.

Van Otterloo, J., Raveggi, M., Cas, R. A. F. & Maas, R. (2014). Polymagmatic activity at the monogenetic Mt Gambier volcanic complex in the Newer Volcanics Province, SE Australia: new insights into the occurrence of intraplate volcanic activity in Australia. *Journal of Petrology* **55**, 1317–1351.

Veevers, J. J. (1986). Breakup of Australia and Antarctica estimated as mid-Cretaceous (95 $\pm$ 5 Ma) from magnetic and seismic data at the continental margin. *Earth and Planetary Science Letters* **77**, 91–99.

Vogel, D. C. & Keays, R. R. (1997). The petrogenesis and platinum-group element geochemistry of the Newer Volcanic Province, Victoria, Australia. *Chemical Geology* **136**, 181–204.

Vollmer, R. (1976). Rb–Sr and U–Th–Pb systematics of alkaline rocks: the alkaline rocks from Italy. *Geochimica et Cosmochimica Acta* **40**, 283–295.

Walter, M. J. (1998). Melting of garnet peridotite and the origin of komatiite and depleted lithosphere. *Journal of Petrology* **39**, 29–60.

Wellman, P. (1974). Potassium–argon ages on the Cainozoic volcanic rocks of Eastern Victoria, Australia. *Journal of the Geological Society of Australia* **21**, 359–376.

Wellman, P. & McDougall, I. (1974). Cainozoic igneous activity in eastern Australia. *Tectonophysics* **23**, 49–65.

Yaxley, G. M., Crawford, A. J. & Green, D. H. (1991). Evidence for carbonatite metasomatism in spinel peridotite xenoliths from western Victoria, Australia. *Earth and Planetary Science Letters* **107**, 305–317.

Yaxley, G. M., Kamenetsky, V. S., Green, D. H. & Falloon, T. J. (1997). Glasses in mantle xenoliths from western Victoria, Australia, and their relevance to mantle processes. *Earth and Planetary Science Letters* **148**, 433–446.

Zhang, M., O'Reilly, S. Y. & Chen, D. (1999). Location of Pacific and Indian mid-ocean ridge–type mantle in two time slices: Evidence from Pb, Sr, and Nd isotopes for Cenozoic Australian basalts. *Geology* **27**, 39.

Zindler, A. & Hart, S. R. (1986). Chemical geodynamics. *Annual Review of Earth and Planetary Sciences* **14**, 493–571.